

VELOCITY CENTROIDS AS TRACERS OF THE TURBULENT VELOCITY STATISTICS

ALEJANDRO ESQUIVEL AND A. LAZARIAN

Astronomy Department, University of Wisconsin-Madison, 475 N. Charter St., Madison, WI 53706, USA

Draft version, February 5, 2008

ABSTRACT

We use the results of magnetohydrodynamic (MHD) simulations to emulate spectroscopic observations and use maps of centroids to study their statistics. In order to assess under which circumstances the scaling properties of the velocity field can be retrieved from velocity centroids, we compare two point statistics (structure functions and power-spectra) of velocity centroids with those of the underlying velocity field and analytic predictions presented in a previous paper (Lazarian & Esquivel 2003). We tested a criterion for recovering velocity spectral index from velocity centroids derived in our previous work, and propose an approximation of the early criterion using only the variances of “unnormalized” velocity centroids and column density maps. It was found that both criteria are necessary, however not sufficient to determine if the centroids recover velocity statistics. Both criteria are well fulfilled for subsonic turbulence. We find that for supersonic turbulence with sonic Mach numbers $\mathcal{M}_s \gtrsim 2.5$ centroids fail to trace the spectral index of velocity. Asymptotically, however, we claim that recovery of velocity statistics is always possible provided that the density spectrum is steep and the observed inertial range is sufficiently extended. In addition, we show that velocity centroids are useful for anisotropy studies and determining the direction of magnetic field, even if the turbulence is highly supersonic, but only if it is sub-Alfvénic. This provides a tool for mapping the magnetic field direction, and testing whether the turbulence is sub-Alfvénic or super-Alfvénic.

Subject headings: ISM: general — ISM: structure — MHD — radio lines: ISM — turbulence

1. INTRODUCTION

It is well established that the interstellar medium (ISM) is turbulent. From the theoretical point of view this arises from the very large Reynolds numbers present in the ISM (the Reynolds number is defined as the inverse ratio of the dynamical timescale -or *eddy turnover time*- to the viscous damping timescale). From an observational standpoint there is also plenty of evidence that supports a turbulent ISM, where the turbulence expands over scales that range from Au to kpc (Larson 1992; Armstrong, Rickett & Spangler 1995; Deshpande, Dwarakanath, & Goss 2000; Stanimirović & Lazarian 2001). This turbulence is very important for many physical processes, including star formation, cosmic ray propagation, heat transport, and heating of the ISM (for a review see Vázquez-Semadeni et al. 2000; Cho & Lazarian 2005; and references therein).

How to compare interstellar turbulence with the results of numerical simulations and theoretical expectations is an important question that must be addressed. After all, theoretical constructions involve necessary simplifications, while numerical simulations of turbulence involve Reynolds, and magnetic Reynolds numbers that are very different from those in the ISM. Are numerical simulations of ISM of value? To what extent do they reproduce interstellar turbulence? These sort of questions one attempts to answer with observations.

Substantial advances in understanding of scaling of compressible MHD turbulence¹ (see reviews by Cho & Lazarian 2005; Lazarian & Cho 2005, and references therein) allow to provide a direct comparison of the theoretical expectations with observations. How reliable are the turbulence spectra obtained via observations?

Studies of statistics of turbulence have been fruitful us-

ing interstellar scintillations (Narayan & Goodman 1989; Spangler & Gwinn 1990). However this technique is restricted to the study of ionized media, and very importantly to density fluctuations alone (see Cordes 1999). Nowadays, radio spectroscopic observations of neutral media provide us with an enormous amount of data containing information about interstellar turbulence, including a more direct physical quantity to study turbulence: velocity. But the emissivity of a spectral line depends on both the velocity and density fields simultaneously, and the separation of their individual contribution is not trivial. Much effort has been put into this difficult task and several statistical measures have been proposed to extract information of velocity from spectroscopic data (see review by Lazarian 1999). Among the simplest we can mention the use of line-widths (Larson 1981, 1992; Scalo 1984, 1987). Velocity centroids have been around as measure of the velocity field for a long time now (von Hoerner 1951; Munch 1958). And they have been widely used to study turbulence in molecular clouds (Kleiner & Dickman 1985; Dickman & Kleiner 1985; Miesch & Bally 1994).

Power-spectra, correlation, and structure functions have been traditionally, and still are, the most widely used tools to characterize the statistics of emissivity maps. These statistical tools have been used to study the scaling properties of turbulence, e.g. to determine its the spectral index. Recently, more elaborated techniques have been proposed to analyze observational data, such as “ Δ -variance” wavelet transform (Stutzki et al. 1998; Mac Low & Ossenkopf 2000; Ossenkopf & Mac Low 2002). Such techniques can be used to obtain velocity information from spectral data with some advantages, like being less sensitive to the effects of edges or noise. Regardless of the method used, it is usually assumed that the map traces the velocity fluctuations, which as we show below this is not always true. To separate velocity from density contribution “Modified Velocity Centroids” (MVCs) were derived in (Lazarian & Esquivel 2003, hereafter LE03).

Electronic address: esquivel@astro.wisc.edu; lazarian@astro.wisc.edu

¹ This scaling was used to solve important astrophysical problems, for instance, finding the rates of scattering of cosmic rays (Yan & Lazarian 2004) and acceleration of cosmic dust (Yan, Lazarian, & Draine 2004).

There has been an effort in parallel to develop new statistics that trace velocity fluctuations. Here we can mention the “Spectral Correlation Function” -SCF- (Rosolowsky et al 1999; Padoan, Rosolowsky & Goodman 2001), “Velocity Channel Analysis” -VCA- (Lazarian & Pogosyan 2000; Lazarian et al. 2001; Esquivel et al. 2003), MVCs (LE03), and “Velocity Coordinate Spectrum” -VCS- (Lazarian 2004). Both VCA and VCS are good for studies of supersonic turbulence². Although SCF was introduced as an empirical tool, its properties, in what the statistics of turbulence is concerned, can be derived using a general theory in Lazarian & Pogosyan (2004).

Synergy of different techniques is very advantageous for studies of interstellar turbulence. Miville-Deschênes, Levrier & Falgarone (2003b) attempted to test the results obtained with VCA using velocity centroids. However, as we show in the paper, without a reliable criterion of whether velocity centroids reflect the velocity statistics such studies deliver a rather limited insight.

Numerical simulations provide us with an ideal testing ground for the statistical tools available for application to observational data. However we must note that the situation is rather complex. On one hand, real observations depend critically on the physical properties of the object under study, such as variations in the excitation state of the tracer and the radiation transfer within it (see Lazarian & Pogosyan 2004). In addition observational limitations, like finite signal-to-noise ratio and map size, gridding effects, beam pattern, beam error, etc. are also present. On the other hand, numerical simulations have their own limitations, such as finite box size and resolution, numerical viscosity, and the physics available to a particular code. This paper is mostly concerned about the projection effects and the impact of density fluctuations to centroid maps, which are shared by observations and simulations.

In LE03 we studied the maps of velocity centroids as tracers of the turbulent velocity statistics. We derived analytical relations between the two point statistics of velocity centroids and those of the underlying velocity field. We also identified an important term in the structure function of centroids which includes information of density, and that can be extracted from observables. Subtraction of that term can isolate better the velocity contribution, and this yielded to a new measure that we termed “modified velocity centroids” (MVCs). In LE03 we proposed a criterion for determining whether velocity centroids reflect the scaling properties of underlying turbulent velocity (e.g. structure functions or spectra of velocity). A major goal of this paper is to test the predictions in LE03 using synthetic maps obtained via MHD simulations and to determine when velocity centroids indeed reflect the velocity statistics.

Earlier on, in Lazarian, Pogosyan & Esquivel (2002) we showed how velocity centroids can be used to reveal the anisotropy of MHD turbulence and how this anisotropy can be used for studies of plane-of-sky magnetic field. This technique was further discussed by Vestuto, Ostriker & Stone (2003). In this paper we show how Mach number and Alfvén Mach number affect the anisotropy of velocity centroid statistics.

The results of LE03 obtained in terms of structure functions are trivially recasted in terms of spectra and correlation functions. Therefore we use structure, correlation functions and

spectra interchangeably through our paper, depending what measure is more convenient. While being interchangeable, for practical statistical data handling different measures have their own advantages and disadvantages. We discuss those on the example of power-law scalar field and thus benchmark our further velocity centroid study. We also deal with a potentially pernicious issue of non-uniformity of notations and normalizations that plague the relevant literature by having details of our derivations in the appendixes that constitute an important part of the paper.

In this work we perform a detailed numerical study of the ability of velocity centroids to extract turbulent velocity statistics. We study the issues of velocity-density correlations and outline the relation of velocity centroids to other techniques. In §2 we review the basic problem of the density and velocity contributions to spectroscopic observations. We summarize LE03 in §3, we include in this work appendixes with mathematical derivations omitted in our earlier short communication. In §4 we test the analytical predictions, and the spectral indices from our numerical data. In §5 we show how centroids can be used for turbulence anisotropy studies and determination of the plane-of-sky direction of magnetic field. A discussion of the results can be found in §6, and a summary in §7.

2. TURBULENCE STATISTICS AND SPECTRAL LINE DATA

Due to the stochastic nature of turbulence it is best described by statistical measures. Among these we have two point statistics such as structure functions, correlation functions, and power spectra (see for instance Monin & Yaglom 1975). Their definition and a more comprehensive discussion can be found in Appendix A. Structure and correlation functions depend in general on a “lag” \mathbf{r} , the separation between two points \mathbf{x}_1 and \mathbf{x}_2 , such that $\mathbf{r} = \mathbf{x}_2 - \mathbf{x}_1$. Power spectrum is defined as the Fourier Transform of the correlation function, and is function of the wave-number vector \mathbf{k} . With amplitude $k = |\mathbf{k}| \sim 2\pi/r$, where $r = |\mathbf{r}|$. Additional simplification is achieved if the turbulent field is isotropic, in which case structure and correlation functions depend only on the magnitude of the separation r (and not on the direction), similarly power spectrum is only function of k . This is not strictly true for magnetized media, as the presence of a magnetic field introduces a preferential direction for motion. In fact, MHD turbulence becomes axisymmetric in a system of reference defined by the direction of the *local* magnetic field (see reviews by Cho & Lazarian 2005 and Cho, Lazarian & Vishniac 2003), thus breaking the isotropy. However, since the local direction changes from one place to another, the anisotropy is rather modest and it is still possible to characterize the turbulence with isotropic statistics (see Esquivel et al. 2003).

2.1. Three-dimensional power-law statistics

In the simplest realization of turbulence we have injection of energy at the largest scales. The energy cascades down without losses to the small scales, at which viscous forces become important and turbulence is dissipated. At intermediate scales, between the injection and the dissipation scales, the turbulent cascade is *self-similar*. This range constitutes the so called *inertial-range*. There the physical variables are proportional to simple powers of eddy sizes, and the two point statistics can be described by power-laws. For power-law statistics Lazarian & Pogosyan (2000) discussed two regimes, a *short-wave-dominated* regime, corresponding to a *shallow*

² Using species heavier than hydrogen one can study subsonic turbulence as well

spectrum, and a *long-wave-dominated* spectrum, with a *steep* spectrum.

While dealing with numerical data one encounters a few non-trivial effects that we find advantageous to discuss below. The insight into the limitations of numerical procedures that involve conversion from mathematically equivalent statistics helps us for the rest of the paper.

2.1.1. Steep (long-wave-dominated) spectrum

Consider an isotropic power-law one-dimensional power-spectrum of the form

$$P_{1D}(k) = C k^{\gamma_{1D}}. \quad (1)$$

A *steep* spectrum corresponds to spectral indices $\gamma_{1D} < -1$. The structure function $D(r)$ can be written in terms of the spectrum as

$$D(r) = 4 \int_0^\infty [1 - \cos(kr)] P_{1D}(k) dk. \quad (2)$$

For a power-law steep power spectrum (substituting eq.[1] into eq.[2]), the structure function also follows a power-law:

$$D(r) = A r^\xi = A r^{-\gamma_{1D}} \quad 0 < \xi < 2, \quad (3)$$

where $A = C 2\pi / [\Gamma(1+\gamma) \sin(\pi\gamma/2)]$, and $\Gamma(x)$ is the Euler Gamma function. The relation between the spectral index of the structure function and power spectrum can be generalized for isotropic fields to $P_{ND} \propto k^{\gamma_{ND}}$, with

$$\gamma_{ND} = -N - \xi. \quad (4)$$

Where N is the number of dimensions (see Appendix A). For instance, the velocity (v) in Kolmogorov turbulence scales as $v \propto r^{1/3}$, which corresponds to a spectral index for the structure function of $\xi = 2/3$, to a three-dimensional power-spectrum (P_{3D}) index $\gamma_{3D} = -11/3$, a two-dimensional power-spectrum (P_{2D}) index $\gamma_{2D} = -8/3$, and a one-dimensional power-spectrum P_{1D} index $\gamma_{1D} = -5/3$. Note that Kolmogorov spectrum falls into the steep spectra category.

Structure functions given by equation (3) are well defined only for $\xi > 0$, which allows to satisfy $D(0) = 0$, and $\xi < 2$, so that the representation in terms of Fourier integrals is possible (see Monin & Yaglom 1975).³

To illustrate the relation between the two point statistics and power-law spectrum, as well as the difficulties associated with handling numerical data. We produced a three-dimensional Gaussian cube with a prescribed (3D) spectral index of $\gamma_{3D} = -11/3$, as described in Esquivel et al. (2003). This type of data-cubes are somewhat similar to the fractional Brownian motion (fBms) fields used by Brunt & Heyer (2002a), or the *de-phased* fields used in Brunt et al. (2003). However, as in real observations, they do not have perfect power-law spectrum for a particular realization, but only in a statistical sense (see Esquivel et al. 2003). In Figure 1 we show the calculated 3D power spectrum, structure and correlation functions of our steep Gaussian cube, and compare them with the prescribed scaling properties. The power spectrum is computed using Fast Fourier Transform (FFT) in 3D and then averaged in wave-number k . Ideally one can compute directly in real space the 3D structure or correlation functions, however for a

³ Correlation functions in this regime are maximal, and finite at $r = 0$. It is important to notice also that for a power-law steep spectrum the structure function is a power-law, but the correlation function is not (see eq. [A4]). The correlation function is a constant minus a growing (positive index) power-law, therefore in a log-log scale is flat at small scales, and drops at large scales.

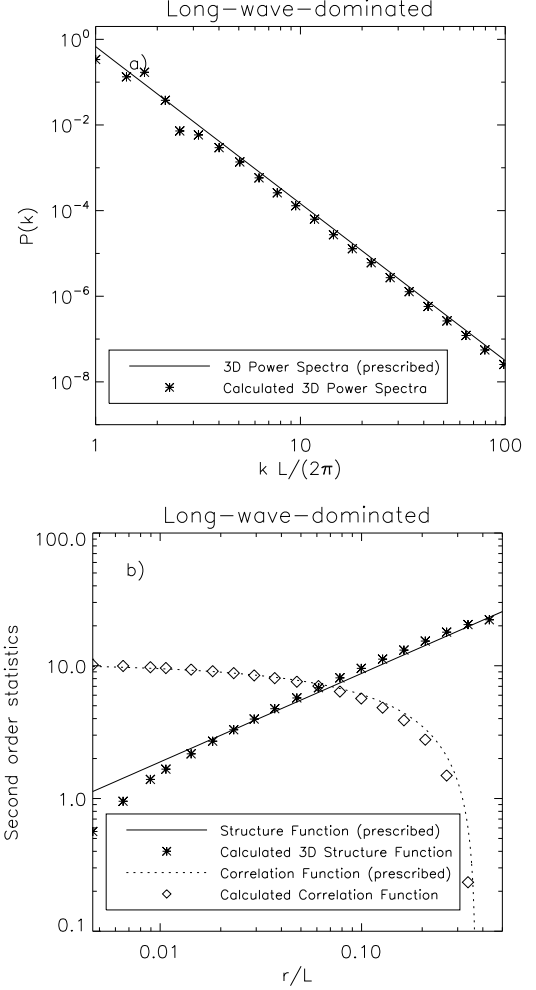


FIG. 1.— Three-dimensional two point statistics of a long-wave dominated Gaussian field (steep spectrum). In panel (a) the three-dimensional power spectrum, the solid line is the prescribed spectrum, with a spectral index of $\gamma_{3D} = -11/3$, the stars correspond to the calculated. In panel (b) the expected structure function (solid line), the computed structure function (stars); the expected correlation function of fluctuations (dotted line), and the calculated correlation function of fluctuations (diamonds).

3D field of the dimensions used here (216^3) is already quite expensive computationally. It would require looping over all the points in the data-cube to do the average and repeat for all the possible values for the lag (in three dimensions as well). Fortunately, since the data-cubes were produced using FFT we can safely compute the correlation function with spectral methods. The correlation function can be expressed as a convolution integral $B(r) \propto \int dr' f(r)f(r+r')$, which can be calculated as a simple product of the Fourier transformed fields. That is, $B(r) \propto \mathcal{F}\{\hat{f}(k) \hat{f}^*(k)\}$, where $\hat{f}(k) = \mathcal{F}\{f(r)\}$ is the Fourier transform of $f(r)$, and $\hat{f}^*(k)$ its complex conjugate. Then, with the use of equation (A4) we can obtain the structure function. The resulting correlation and structure functions in 3D are then averaged in r . An important thing to notice is that the Gaussian cubes have wrap-around periodicity, and the largest variation available correspond to scales of $L/2$, where L is the size of the computational box. In fact, we only plot the structure and correlation functions up to such separations. We see a fair agreement with prescribed and the measured scaling properties. The power spectrum in Figure 1(a) shows departures from strict power-law which are more

evident for small wave-numbers. This is natural for this type of data-cubes, where random deviations from strict power-law are expected at all scales. But at large scales (small k) we have fewer points for the statistics and the departures do not average to zero, while at small scales they almost do.

2.1.2. Shallow (short-wave-dominated) spectrum

When the energy spectrum is shallow (i.e. $\gamma_{1D} > -1$), the fluctuations of the field are dominated by small-scales, therefore termed *short-wave-dominated* regime. Density at high Mach number is an example of such shallow spectrum (see Beresnyak, Lazarian & Cho 2005). In this case neither the structure nor correlation functions can be strictly represented by power-laws. In fact, in order for the Fourier Transforms to converge in this case we need to introduce a cutoff for small wave-numbers, such that the power spectrum is only a power-law for $k > k_0$, in other words

$$P_{1D}(k) = C' (k_0^2 + k^2)^{\gamma_{1D}/2} = C' (k_0^2 + k^2)^{(-\eta-1)/2}. \quad (5)$$

To a power spectrum of this form corresponds a correlation function of fluctuations:

$$\tilde{B}(r) = A' \left(\frac{r}{r_c} \right)^{\eta/2} K_{\eta/2} \left(\frac{2\pi r}{r_c} \right), \quad (6)$$

where, $r_c = 2\pi/k_0$, $K_\eta(x)$ is the η -order, modified Bessel function of the second kind (also sometimes referred as hyperbolic Bessel function), and $A' = C' 2^{1-\eta} \pi^{-(\eta+1)/2} r_c^\eta / \Gamma[(\eta+1)/2]$. The N th-dimensional power spectrum index for a correlation function of the form $B \propto (r/r_c)^{\eta/2} K_{\eta/2}(2\pi r/r_c)$ can also be generalized to $P_{ND} \propto (k_0^2 + k^2)^{\gamma_{ND}/2}$, with

$$\gamma_{ND} = -N - \eta. \quad (7)$$

This relation is very similar to that for the long wave dominated case (eq[4]). Actually for $r \ll r_c$, $K_{\eta/2}$ can be expanded as $\sim (r/r_c)^{\eta/2}$, thus the 3D correlation function (as opposed to the structure function as in the long wave dominated regime) goes as a power-law $\tilde{B}(r) \sim (r/r_c)^\eta$ for small separations. Notice that for a shallow spectrum the structure function grows rapidly at the smallest scales and then flattens. Similarly to the steep spectrum, we produced a short-wave-dominated Gaussian 3D field, with a prescribed index of $\gamma_{3D} = -2.5$. In Figure 2 we present the expected, and calculated two point statistics. Here the critical scale r_c is determined by the smallest wave-number ($k_0 = 2\pi/L$), in our case it corresponds to the size of the computational box ($r_c = L$). We see again a fair agreement with the prescribed and calculated spectra. However, Figure 2 reveals a significant departure of the calculated correlation function with the prediction from equation (6) for large lags. The explanation of such difference is that the analytical relations of spectra (eqs. [1, 5]) with structure and correlation functions (eqs. [3, 6]) is exact only in the limit of continuous integrals over infinite wave-numbers. The data-sets presented in this section are constructed in Fourier space, then translated to real space by means of discrete Fourier transforms of the form:

$$\tilde{u}(x) = \sum_{k=1}^{L-1} |P_{1D}(k)|^{1/2} \exp[2\pi kx/L] \quad (8)$$

The sum runs from $k = 1$ ensuring that $\langle \tilde{u}(x) \rangle = 0$. In practice, we evaluate the Fourier Transforms via FFT and set explicitly the $k = 0$ component of the spectrum to zero to guarantee that

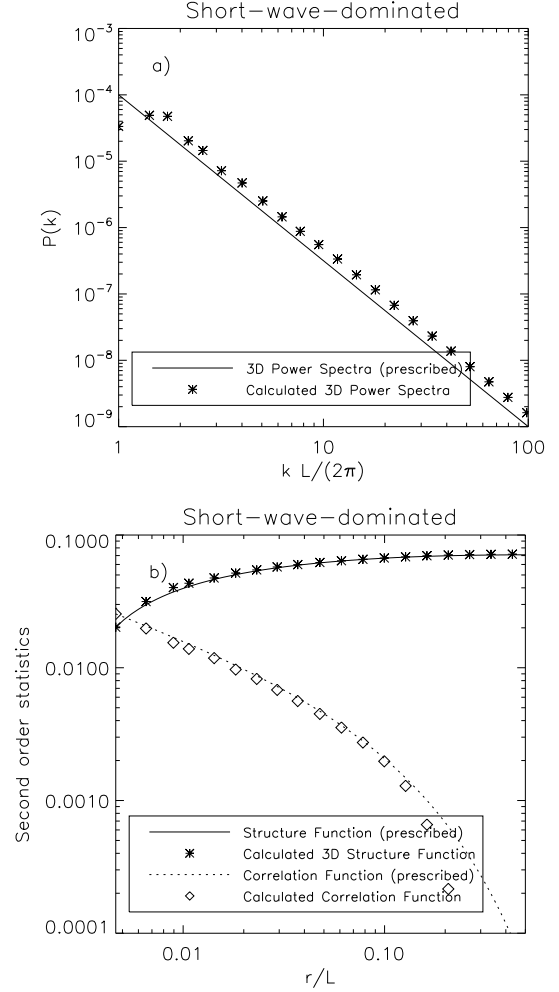


FIG. 2.— Same as Fig. 1 but for a short-wave dominated spectrum (3D spectral index of $\gamma_{3D} = -2.5$).

the average of the fluctuating part of the field is null. The resulting field has a limited range of harmonics available, determined basically by the computational grid size (L). We have constructed large 1D fields, in which we see that the gap between the analytical and the computed correlation functions gets smaller as we increase resolution. Thus, it is not surprising that spectra shows a much better correspondence than correlation functions. At the same time, structure functions do not deal with the lowest harmonics, which introduce largest errors (see Monin & Yaglom 1975). And therefore, they are less affected by the lack of lower harmonics as can be confirmed by the fact that they are closer to the analytical prediction than correlation functions. It is important to always keep in mind the issues that can arise from the discrete nature of the data. However, we must note that this particular problem lies within the generation of the data-sets in frequency space and not in the computation of correlation or structure functions via spectral methods. We obtain identical results using FFT and looping in directly in real space to do the average required. In real life, the limitation is likely to be in the opposite direction: the finite wave-numbers available would show up as uncertainty in determining the power spectra while structure and correlation functions should be estimated with smaller errors (if measured directly in real space).

2.2. Structure functions of quantities projected along the line of sight

From spectroscopic observations we can not obtain either the density or velocity fields in real space (x, y, z), but we have to deal with projections along the line of sight (LOS). Despite the fact that our main goal is to extract velocity statistics from the centroids of velocity, we will discuss in this section the statistics of density integrated along the LOS (column density). It will become clear later that the same procedure can be applied to obtain velocity statistics. The issue of projection has been previously discussed in Lazarian (1995), here we briefly state some results that are relevant to this work. In Appendix B we exemplify the projection effects of structure functions for the particular case of power-law statistics. And in Appendix C the power-spectrum of a homogeneous field that has been integrated along the LOS.

In what follows we will assume that the emissivity of our medium is proportional to the first power of the density (this is true, for instance, in the case of H I). We will consider an isothermal medium, and neglect the effects of self-absorption. In this case the integrated intensity of the emission (integrated along the velocity coordinate) is proportional to the column density (see Appendix A for more details):

$$I(\mathbf{X}) \equiv \int \alpha \rho_s(\mathbf{X}, v_z) dv_z = \int \alpha \rho(\mathbf{x}) dz, \quad (9)$$

where α is a constant and $\rho(\mathbf{x})$ is the mass density. The density of emitters $\rho_s(\mathbf{X}, v_z)$ can be identified as the column density per velocity interval, commonly referred as dN/dv . To distinguish between 2D and 3D vectors, we will use capital letters to denote the former and lower case for the latter (i.e. $\mathbf{X} = [x, y]$, $\mathbf{x} = [x, y, z]$). Our assumption is satisfied for observational data where the medium is optically thin, thermalized, and with constant excitation conditions. However, for any observed map its applicability has to be examined carefully. Even for H I widespread self-absorption has been detected (for example Jackson et al. 2002; Li & Goldsmith 2003).

Consider the structure function of the integrated intensity described in equation (9)

$$\langle [I(\mathbf{X}_1) - I(\mathbf{X}_2)]^2 \rangle = \left\langle \left(\int_0^{z_{tot}} \alpha \rho(\mathbf{x}_1) dz - \int_0^{z_{tot}} \alpha \rho(\mathbf{x}_2) dz \right)^2 \right\rangle, \quad (10)$$

where we have written explicitly the limits of integration, with z_{tot} being the size of the object (in the LOS direction). Clearly z_{tot} does not necessarily have to coincide with the transverse size (in the plane of the sky) of the object under study, however that is the case in our data-sets. As described in Lazarian (1995), we can expand the square in equation (10) combining

$$\left(\int \chi(x) dx \right)^2 = \iint \chi(x_1) \chi(x_2) dx_1 dx_2, \quad (11)$$

and the elementary identity

$$(a-b)(c-d) = \frac{1}{2} \left[(a-d)^2 + (b-c)^2 - (a-c)^2 - (b-d)^2 \right], \quad (12)$$

to obtain

$$\langle [I(\mathbf{X}_1) - I(\mathbf{X}_2)]^2 \rangle = \alpha^2 \int_0^{z_{tot}} \int_0^{z_{tot}} dz_1 dz_2 \left[d_\rho(\mathbf{r}) - d_\rho(\mathbf{r})|_{\mathbf{x}_1=\mathbf{x}_2} \right]. \quad (13)$$

Where $d_\rho(\mathbf{r})$ is the 3D structure function of the density,

$$d_\rho(\mathbf{r}) = \langle [\rho(\mathbf{x}_1) - \rho(\mathbf{x}_2)]^2 \rangle. \quad (14)$$

This definition is general and does not require any particular functional form of the 3D structure functions (i.e. power-law statistics). The problem of formally inverting equation (13) to obtain the underlying statistics, allowing for anisotropic turbulence, with an arbitrary spectrum (i.e. not a power-law), has been presented in Lazarian (1995), but it is somewhat mathematically involved. For 3D fields with a power-law spectrum, homogeneous and isotropic, the structure functions of the integrated fields (2D maps) can be simply approximated by two power-laws, one at small the other at large separations (see Minter 2002, and also Appendix B). For instance, if the density has a power-spectrum $P_{3D,\rho} \propto k^{\gamma_{3D}}$, the structure function of column density will have the form

$$\langle [I(\mathbf{X}_1) - I(\mathbf{X}_2)]^2 \rangle \propto R^\mu, \quad (15)$$

where R is the separation in the plane of the sky ($R = |\mathbf{R}| = |\mathbf{X}_2 - \mathbf{X}_1|$), and

$$\mu \approx \begin{cases} -\gamma_{3D} - 2 & \text{for } R \ll z_{tot} \text{ (either steep or shallow spectrum),} \\ -\gamma_{3D} - 3 & \text{for } R \gg z_{tot}, \text{ and } \gamma_{3D} < -3 \text{ (steep spectrum),} \\ 0 & \text{for } R \gg z_{tot}, \text{ and } \gamma_{3D} > -3 \text{ (shallow spectrum).} \end{cases} \quad (16)$$

In contrast, the power spectrum of a field integrated along the LOS corresponds to selecting only the $k_{LOS} = 0$ components of the underlying 3D spectra, more precisely only the solenoidal part (see Appendix C). Thus, for isotropic and homogeneous power-law statistics the 2D power spectrum will reflect the 3D spectral index. If for instance the density has a power spectrum $P_{3D,\rho} \propto k^{\gamma_{3D}}$, the spectrum of column density will scale as

$$P_{2D,I} \propto K^{\gamma_{3D}}. \quad (17)$$

We computed spectra and structure functions for the Gaussian cubes used before, integrated along the z direction. And presented them in Figure 3 along with the expected behavior from eqs.(16) and (17). For the structure functions we show only the asymptotic behavior for small separations ($R \ll z_{tot}$) as the $R \gg z_{tot}$ scales are unavailable (the maximum scale not affected by wrap-around periodicity is $L/2 = z_{tot}/2$).

If the LOS size of the object under study is much smaller than its size in the plane of the sky (so $R \gg z_{tot}$ is possible) we would see the underlying 3D spectral index of the structure functions for large separations (i.e. no projection effect). With enough resolution we could use the 2D spectral index of the column density map for $R \ll z_{tot}$ to infer the underlying 3D index of the density. However, for the resolution used here (216^3 pixels), the projected structure function for small lags is already in the transition between the two asymptotics in eq.[16]. Thus the measured index of the projected map is always shallower (smaller) than the actual $\mu \approx -\gamma_{3D} - 2$. Another subtle, yet interesting point, is that power spectrum applied to map of integrated velocity field, such as

$$V_z(\mathbf{X}) = \int v_z(\mathbf{x}) dz \quad (18)$$

will recover only the incompressible (solenoidal) component of the field. This could be potentially used to study the role of compressibility in turbulence statistics, by combining velocity centroids and VCA (LE03).

3. MODIFIED VELOCITY CENTROIDS REVISITED.

Velocity centroids have been widely used to relate their statistics with velocity, their conventional form is (Munch

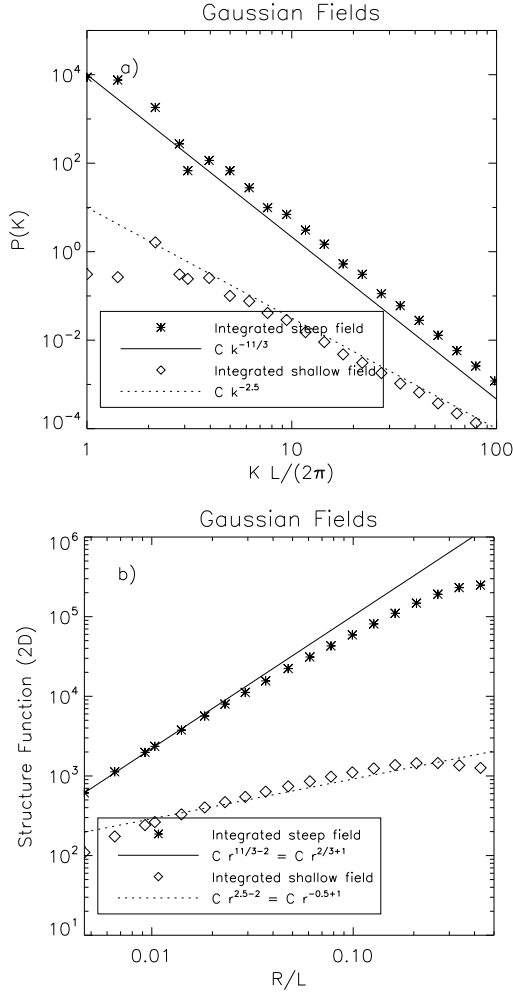


FIG. 3.— Two point statistics for Gaussian fields integrated along the z direction. In panel (a) we show the 2D power spectra, panel (b) correspond to the second order structure functions. The stars correspond to a steep spectrum with a prescribed 3D power spectrum index of $\gamma_{3D} = -11/3$, the diamonds correspond to a shallow spectrum with a prescribed 3D power spectrum index of $\gamma_{3D} = -2.5$. In solid and dotted lines respectively, we plotted for reference the expectations for both long-wave or short-wave dominated cases. The vertical scales in panel (b) have been modified arbitrarily for visual purposes.

1958)

$$C(\mathbf{X}) = \frac{\int v_z \rho_s(\mathbf{X}, v_z) dv_z}{\int \rho_s(\mathbf{X}, v_z) dv_z}. \quad (19)$$

We will refer to this definition as “normalized” centroids. The denominator in equation (19) introduces an extra algebraic complication for a direct analytical treatment of the two-point statistics. For the sake of simplicity we start considering “unnormalized” velocity centroids:

$$S(\mathbf{X}) = \int \alpha v_z \rho_s(\mathbf{X}, v_z) dv_z \quad (20)$$

(notice that they have units of density times velocity as opposed to velocity alone).

Similarly to the expression in equation (9), with emissivity proportional to the first power of the density, and no self absorption, the structure function of the unnormalized velocity

centroids is:

$$\langle [S(\mathbf{X}_1) - S(\mathbf{X}_2)]^2 \rangle = \left\langle \left(\alpha \int v_z(\mathbf{x}_1) \rho(\mathbf{x}_1) dz - \alpha \int v_z(\mathbf{x}_2) \rho(\mathbf{x}_2) dz \right)^2 \right\rangle. \quad (21)$$

Presenting the density and velocity as a sum of a mean value and a fluctuating part: $\rho = \rho_0 + \tilde{\rho}$, $v_z = v_0 + \tilde{v}_z$. Where $\rho_0 = \langle \rho \rangle$, $v_0 = \langle v_z \rangle$, and the fluctuations satisfy $\langle \tilde{\rho} \rangle = 0$, $\langle \tilde{v}_z \rangle = 0$. Analogous to equation (13), the structure function of the unnormalized centroids can be written as

$$\langle [S(\mathbf{X}_1) - S(\mathbf{X}_2)]^2 \rangle = \alpha^2 \iint dz_1 dz_2 [D(\mathbf{r}) - D(\mathbf{r})|_{\mathbf{x}_1=\mathbf{x}_2}], \quad (22)$$

with

$$D(\mathbf{r}) = \langle [v_z(\mathbf{x}_1)\rho(\mathbf{x}_1) - v_z(\mathbf{x}_2)\rho(\mathbf{x}_2)]^2 \rangle. \quad (23)$$

And $D(\mathbf{r})$ can be approximated as:

$$D(\mathbf{r}) \approx \langle v_z^2 \rangle d_\rho(\mathbf{r}) + \langle \rho^2 \rangle d_{v_z}(\mathbf{r}) - \frac{1}{2} d_\rho(\mathbf{r}) d_{v_z}(\mathbf{r}) + c(\mathbf{r}), \quad (24)$$

which includes the underlying 3D structure function of the LOS velocity

$$d_{v_z}(\mathbf{r}) = \langle [v_z(\mathbf{x}_1) - v_z(\mathbf{x}_2)]^2 \rangle, \quad (25)$$

and cross-correlations of velocity and density fluctuations⁴:

$$c(\mathbf{r}) = 2 \langle \tilde{v}_z(\mathbf{x}_1) \tilde{\rho}(\mathbf{x}_2) \rangle^2 - 4\rho_0 \langle \tilde{\rho}(\mathbf{x}_1) \tilde{v}_z(\mathbf{x}_1) \tilde{v}_z(\mathbf{x}_2) \rangle. \quad (26)$$

Because the derivation of equations (22), (24), and (26) involves some tedious algebra, we place it in Appendix D. With all of this, the structure function of unnormalized velocity centroids can be decomposed as

$$\langle [S(\mathbf{X}_1) - S(\mathbf{X}_2)]^2 \rangle = I1(\mathbf{R}) + I2(\mathbf{R}) + I3(\mathbf{R}) + I4(\mathbf{R}), \quad (27)$$

where

$$I1(\mathbf{R}) = \alpha^2 \langle v_z^2 \rangle \iint dz_1 dz_2 [d_\rho(\mathbf{r}) - d_\rho(\mathbf{r})|_{\mathbf{x}_1=\mathbf{x}_2}], \quad (28)$$

$$I2(\mathbf{R}) = \alpha^2 \langle \rho^2 \rangle \iint dz_1 dz_2 [d_{v_z}(\mathbf{r}) - d_{v_z}(\mathbf{r})|_{\mathbf{x}_1=\mathbf{x}_2}], \quad (29)$$

$$I3(\mathbf{R}) = -\frac{1}{2} \alpha^2 \iint dz_1 dz_2 [d_\rho(\mathbf{r}) d_{v_z}(\mathbf{r}) - d_\rho(\mathbf{r})|_{\mathbf{x}_1=\mathbf{x}_2} d_{v_z}(\mathbf{r})|_{\mathbf{x}_1=\mathbf{x}_2}], \quad (30)$$

$$I4(\mathbf{R}) = \alpha^2 \iint dz_1 dz_2 [c(\mathbf{r}) - c(\mathbf{r})|_{\mathbf{x}_1=\mathbf{x}_2}]. \quad (31)$$

With this new decomposition is more evident the definition of the structure function of “modified” velocity centroids (MVCs), which is

$$\begin{aligned} M(\mathbf{R}) &= \langle [S(\mathbf{X}_1) - S(\mathbf{X}_2)]^2 \rangle - \langle v_z^2 \rangle [I(\mathbf{X}_1) - I(\mathbf{X}_2)]^2 \\ &= \langle [S(\mathbf{X}_1) - S(\mathbf{X}_2)]^2 \rangle - I1(\mathbf{R}) \\ &= I2(\mathbf{R}) + I3(\mathbf{R}) + I4(\mathbf{R}). \end{aligned} \quad (32)$$

The velocity dispersion $\langle v_z^2 \rangle$ can be obtained directly from observations using the second moment of the spectral lines

$$\langle v_z^2 \rangle \equiv \frac{\int v_z^2 \rho_s(\mathbf{X}, v_z) dv_z}{\int \rho_s(\mathbf{X}, v_z) dv_z}. \quad (33)$$

Thus also $I1(\mathbf{R})$, which can be related to the structure function of column density as $I1(\mathbf{R}) = \langle v_z^2 \rangle \langle [I(\mathbf{X}_1) - I(\mathbf{X}_2)]^2 \rangle$.

⁴ Note that equation (26) is somewhat different from LE03, where there was a misprint; which has no effect on the results presented.

Similarly, the power spectrum of centroids can be decomposed as (details in Appendix F):

$$P_{2D,S}(\mathbf{K}) = \langle \rho^2 \rangle \langle v_z^2 \rangle (\alpha z_{tot})^2 \delta(\mathbf{K}) + v_0^2 P_{2D,I}(\mathbf{K}) + \alpha^2 \rho_0^2 P_{2D,V_z}(\mathbf{K}) + \mathcal{F}\{B3(\mathbf{R})\} + \mathcal{F}\{B4(\mathbf{R})\}. \quad (34)$$

The term $\langle \rho^2 \rangle \langle v_z^2 \rangle (\alpha z_{tot})^2 \delta(\mathbf{R})$ has no effect in the slope of the power spectrum because it only has power at $\mathbf{K} = \mathbf{0}$. $P_{2D,I}(\mathbf{K})$, and $P_{2D,V_z}(\mathbf{K})$ are the spectra of column density, and integrated velocity respectively. They can be used to obtain the 3D spectral index of density (or velocity) as shown in Appendix C. $\mathcal{F}\{B3(\mathbf{R})\}$ is the Fourier transform of $B3(\mathbf{R})$, a cross-term term analogous to $I3(\mathbf{R})$, but in terms of correlation functions. Similarly, $\mathcal{F}\{B4(\mathbf{R})\}$ include the same density-velocity cross-correlations as $I4(\mathbf{R})$.

The power spectrum of MVCs can be obtained by subtracting $\langle v_z^2 \rangle P_{2D,I}(\mathbf{K})$ from the spectrum of centroids. We derive in Appendix G a criterion for MVCs to trace the statistics of velocity better than unnormalized centroids. It was found that, with very little dependence on the spectral index, MVCs are advantageous compared to unnormalized centroids at small lags. This result is general and we tested it using analytical expressions for the structure functions. For simplicity we considered only the two physically motivated cases, steep density with steep velocity, and shallow density with steep velocity. The latter was not included explicitly in Appendix G because we obtain almost identical results in both cases.

If $v_0 = 0$ and $\mathcal{F}\{B3(\mathbf{R})\} + \mathcal{F}\{B4(\mathbf{R})\}$ can be neglected the spectrum of unnormalized centroids will trace the solenoidal component of the underlying velocity spectrum ($F_{NN}[K, 0]$, see Appendix C). But if the turbulent velocity field is mostly solenoidal, as supported by numerical simulations (Matthaeus et al. 1996; Porter, Woodward & Pouquet 1998; Cho & Lazarian 2003), the power-spectrum is uniquely defined assuming isotropy ($E(k) = \int P_{ND}(\mathbf{k}) d\mathbf{k} \approx 4\pi k^2 F_{NN}[k]$). In the same way if $I1(\mathbf{R})$ can be eliminated (either for being small compared to the structure function of centroids or by subtraction -MVCs-) and if $I2(\mathbf{R}) \gg I3(\mathbf{R}) + I4(\mathbf{R})$, the structure function of the remaining map will trace the structure function of a map of integrated turbulent velocity. And we can in principle recover the underlying 3D velocity statistics (see Appendix B). With this background (and disregarding the cross-terms $I3[\mathbf{R}]$, $I4[\mathbf{R}]$) we arrived in LE03 to a criterion for safe use of (unnormalized) velocity centroids: if

$$\langle [S(\mathbf{X}_1) - S(\mathbf{X}_2)]^2 \rangle \gg \langle v_z^2 \rangle \langle [I(\mathbf{X}_1) - I(\mathbf{X}_2)]^2 \rangle, \quad (35)$$

then the structure function of velocity centroids will mostly trace the turbulent velocity statistics, otherwise the density fluctuations are important and will be reflected in the centroid measures. When the structure function of velocity centroids is shallower or at least not much steeper than that of the column density, which can be verified by the power spectrum, or computing the structure function directly in 3D for a few of values for the lag. Then the criterion proposed in LE03 can be simplified to use only the variances of the two maps (and the velocity dispersion):

$$\langle \tilde{S}^2 \rangle \gg \langle v_z^2 \rangle \langle \tilde{I}^2 \rangle. \quad (36)$$

If any of these two criteria is violated, one could in principle subtract the contribution of density and the MVCs would trace velocity structure function, provided that we could neglect the cross-terms.

The contribution of velocity-density cross-correlations ($c[\mathbf{r}]$) have been studied earlier. For VCA it has been shown to

be marginal (Lazarian et al. 2001; Esquivel et al. 2003). However, a more detailed discussion of their effect in the context of MVCs is necessary, and is provided below.

$I3(\mathbf{R})$ and $\mathcal{F}\{B3(\mathbf{R})\}$ are in some sense “cross-terms”, $I4(\mathbf{R})$ and $\mathcal{F}\{B4(\mathbf{R})\}$ are related to correlations between density and velocity. We expect both pairs to grow as we increase the “interrelation” between density and velocity. We will refer to $I3[\mathbf{R}]$ (or $\mathcal{F}\{B3(\mathbf{R})\}$) simply as “cross-term”, and to $I4[\mathbf{R}]$ (or $\mathcal{F}\{B4(\mathbf{R})\}$) as “cross-correlations” of density-velocity. The latter should be zero for uncorrelated data. At the same time the cross-term can be studied analytically for power-law statistics as presented in Appendix E, and will not be zero, even in the case of uncorrelated velocity and density fields. Before computing them directly, in order to get a feeling of how important the cross-term could become one can consider structure functions. First of all, note that $\langle [S(\mathbf{X}_1) - S(\mathbf{X}_2)]^2 \rangle$ is positive defined, and so are $I1(\mathbf{R})$ and $I2(\mathbf{R})$. The remaining terms can be negative, in which case they must be smaller than the sum of $I1(\mathbf{R})$ and $I2(\mathbf{R})$. Let us focus for the moment on the contribution of $I3(\mathbf{R})$ and disregard cross-correlations between density and velocity. Its magnitude is maximal at large scales, and so are $I1(\mathbf{R})$ and $I2(\mathbf{R})$. At such scales $|I3(\mathbf{R})|$ is on the order of $I1(\mathbf{R})$ and $I2(\mathbf{R})$. However, in $I2(\mathbf{R})$ the structure function of velocity is weighted by $\langle \rho^2 \rangle = \rho_0^2 + \langle \tilde{\rho}^2 \rangle$ instead of only $\langle \tilde{\rho}^2 \rangle$, enhancing the velocity statistics compared to the cross-term. The importance of the cross-term at the small scales (in which we are most interested) will depend on details such as how steep the underlying structure functions are (see Appendix E), and the zero levels of density and velocity (see Ossenkopf et al. 2005). This is easy to understand for a particular case of power-law statistics of the form $d_\rho(r) \propto r^n$, and $d_{v_z}(r) \propto r^m$, with $(m, n > 0)$, i.e. both fields steep). Here the cross-term scales as $\propto r^{m+n}$, steeper than both velocity and density. If at large scales $I1(\mathbf{R})$ and $I2(\mathbf{R})$ are on the order of $|I3(\mathbf{R})|$, provided that the latter falls more rapidly toward small scales, its contribution will be smaller than both velocity and density structure functions, at those scales. But if the density or the LOS velocity (or both), have a shallow spectrum, the cross-term can be larger than $I1(\mathbf{R})$ or $I2(\mathbf{R})$, and can affect significantly the statistics of centroids. Measured spectral indices of density in the literature, range from $\gamma_{3D} \sim -2.5$ to $\gamma_{3D} \sim -4.0$, which include both shallow and steep. This is true for observations in different environments in the ISM (for instance, Deshpande et al. 2000; Bensch, Stutzki & Ossenkopf 2001; Stanimirović & Lazarian 2001; Ossenkopf & Mac Low 2002), as well as for numerical simulations (see Cho & Lazarian 2002; Brunt & Mac Low 2004; Beresnyak et al. 2005). The velocity spectral index is less known from observations, but has been measured to be only in the steep regime (for example using VCA, e.g. in Stanimirović & Lazarian 2001), also in agreement with simulations. From the theoretical standpoint, at small scales when self-gravity is important we might expect clumping that result on enhanced small scale structure (yielding a shallow spectrum). On the other hand there are no clear physical grounds to our knowledge that will produce a small scale dominated (shallow) velocity field. However, even in the simple case of steep density and steep velocity spectra it is not clear beforehand how important density-velocity cross-correlations ($I4[\mathbf{R}]$) could be. Later, we will analyze the contribution of the cross-terms and density-velocity cross-correlations in more detail, including spectra.

TABLE 1
PARAMETERS OF THE FOUR RUNS USED.

Model	B_0	$\langle P_{\text{gas}} \rangle$	β	rms v	\mathcal{M}_s	\mathcal{M}_A	$\langle \tilde{S}^2 \rangle / (\langle v_z^2 \rangle \langle \tilde{P}^2 \rangle)$
A	1.0	2.0	4	< 0.7	~ 0.5	~ 0.7	93.9
B	1.0	0.1	0.2	~ 0.7	~ 2.5	~ 0.7	4.6
C	0.1	0.1	0.2	~ 0.7	~ 2.5	~ 8	4.2
D	1.0	0.01	0.02	~ 0.7	~ 7	~ 0.7	2.2

4. TESTING VELOCITY CENTROIDS NUMERICALLY

In LE03 we performed some preliminary tests of the modified velocity centroids using numerical simulations and compared the power-spectrum with that of velocity field, normalized (equation [19]), and unnormalized centroids (equation [20]). In this section we provide a more detailed test to investigate under what conditions velocity centroids can be used to recover the velocity statistics.

4.1. The data

We took compressible MHD data-cubes from the numerical simulations of Cho & Lazarian (2003). This data-cubes correspond to fully-developed (driven) turbulence. The turbulence is driven in Fourier Space (solenoidally) at wave-numbers $2 \leq (k_{\text{driving}} L / [2\pi]) < 3.4$. The data-cubes have a resolution of 216^3 pixels. We use four sets of simulations, the parameters for each run are summarized in Table 1. The models include various values of the plasma β (ratio of gas to magnetic pressures), sonic Mach numbers \mathcal{M}_s , and Alfvén Mach number \mathcal{M}_A . All of these parameters can be found in the ISM under different situations. For more details about the simulations we refer the reader to Cho & Lazarian (2003). The outcome of the simulations are density and velocity data-cubes that we use to compute the centroids. We will refer to this data-sets as “original”, and the existing correlations between density and velocity (consistent with MHD evolution) are left intact. The numerical simulations have a limited inertial range. We do not have power-law statistics (i.e. inertial range) at the largest scales (smallest wave-numbers) due to the driving of the turbulence. And neither we have power-law statistics at the smallest scales (largest wave-numbers), because of numerical dissipation. Thus, it is very difficult to estimate spectral indices because the measured log-log-slope is quite sensitive to the range in wave-numbers (or lags) used. This poses a problem of obtaining quantitative results. For that reason, we created another data-set by modifying the original fields to have strict power-law spectra, following the procedure in Lazarian et al. (2001). The procedure consists in modifying the amplitude of the Fourier components of the data so they follow a power-law, while keeping the phases intact. This way we preserve most of the spatial information. By keeping the phases we also minimize the effect of the modification to the density-velocity correlations. In addition, these new fields have the same mean value than the original data-sets, and the magnitude of their power-spectra (vertical offset) was fixed to match the original variances as well. We will refer to this data-sets as “reformed”.

4.2. Results

Column density and centroids of velocity are two-dimensional maps, and therefore it is not computationally restrictive to obtain their correlation or structure function directly in real space. Power-spectrum is often computationally

TABLE 2
THREE-DIMENSIONAL SPECTRAL INDICES. THE VALUES IN PARENTHESES CORRESPOND TO THE *original* SIMULATIONS, AND IN BOLD FACE TO THE *reformed* DATA-SETS.

Model	Density		LOS Velocity	
	$-\gamma_{3D}$	m	$-\gamma_{3D}$	m
A	(3.5) 3.5	(0.4) 0.6	(3.8) 3.8	(0.5) 0.8
B	(3.3) 3.3	(0.3) 0.4	(3.6) 3.6	(0.5) 0.6
C	(3.1) 3.1	(0.1) 0.3	(4.0) 4.0	(0.8) 0.9
D	(2.6) 2.6	... *	(3.8) 3.8	(0.6) 0.8

*The measured power-spectrum index in this case corresponds to a *shallow* spectrum. Thus, the correlation function is expected to follow a power-law, not the structure function.

cheaper because FFT can be used. However, inherent difficulties of applying Fourier analysis to real data, for instance the lack of periodic boundary conditions and instrumental response make power spectrum often unreliable. To alleviate this problem more elaborate techniques like wavelet transforms have been proposed (Zielinsky & Stutzki 1999). Moreover, if the observed maps are not naturally arranged in a Cartesian grid one would need to smear the data onto that kind of grid to use FFT. Which is not necessary for structure or correlation functions if computed directly averaging in configuration space. In despite of this, because the simulations we used are in a Cartesian grid and indeed have periodic boundary conditions, we can compute spectra, correlation, and structure functions using FFT (see §2) with as good accuracy than doing the average in real space. The relation between the structure function, correlation function, and power spectrum of unnormalized centroids can be found in Appendix F.

4.2.1. 3D statistics

Before we study the 2D maps and try to extract from those the underlying 3D statistics we will start by computing the three-dimensional statistics. This is shown in Figure 4. It is noticeable that only for the case where the turbulence is subsonic ($\mathcal{M}_s \sim 0.5$) the level of the velocity fluctuations is larger than that of the density. In the figure is also evident the limited inertial range in the original simulations (i.e. not perfect power-law statistics). Spectral indices (log-log slopes), both for power-spectra and structure functions from Figure 4 are given in Table 2. For the original data-sets the indices for power-spectra were obtained in a range of wave-numbers $kL/(2\pi) \sim [5 - 15]$ (between the scale of injection and the scales at which dissipation is dominant). The structure functions spectral indices were calculated with the corresponding values for spatial separations, $r/L \sim [1/15 - 1/5]$. The reformed data-sets were constructed using the power-spectra indices estimated for the original MHD simulations. We can see in Fig. 4 the idealized power-law spectra of the reformed data-sets. At the same time, although structure functions do not have such perfect power-law behavior (see discussion at the end of §2.1), they show improvement compared to the original simulations. The range of scales used to measure the spectral indices for the reformed data-sets is $kL/(2\pi) \sim [3.5 - 100]$ or $r/L \sim [1/100 - 1/3.5]$, much wider than for the original sets. Notice that power-spectra for the density becomes shallower with the increase of the Mach number. At the same time the spectral index of velocity is always steep.

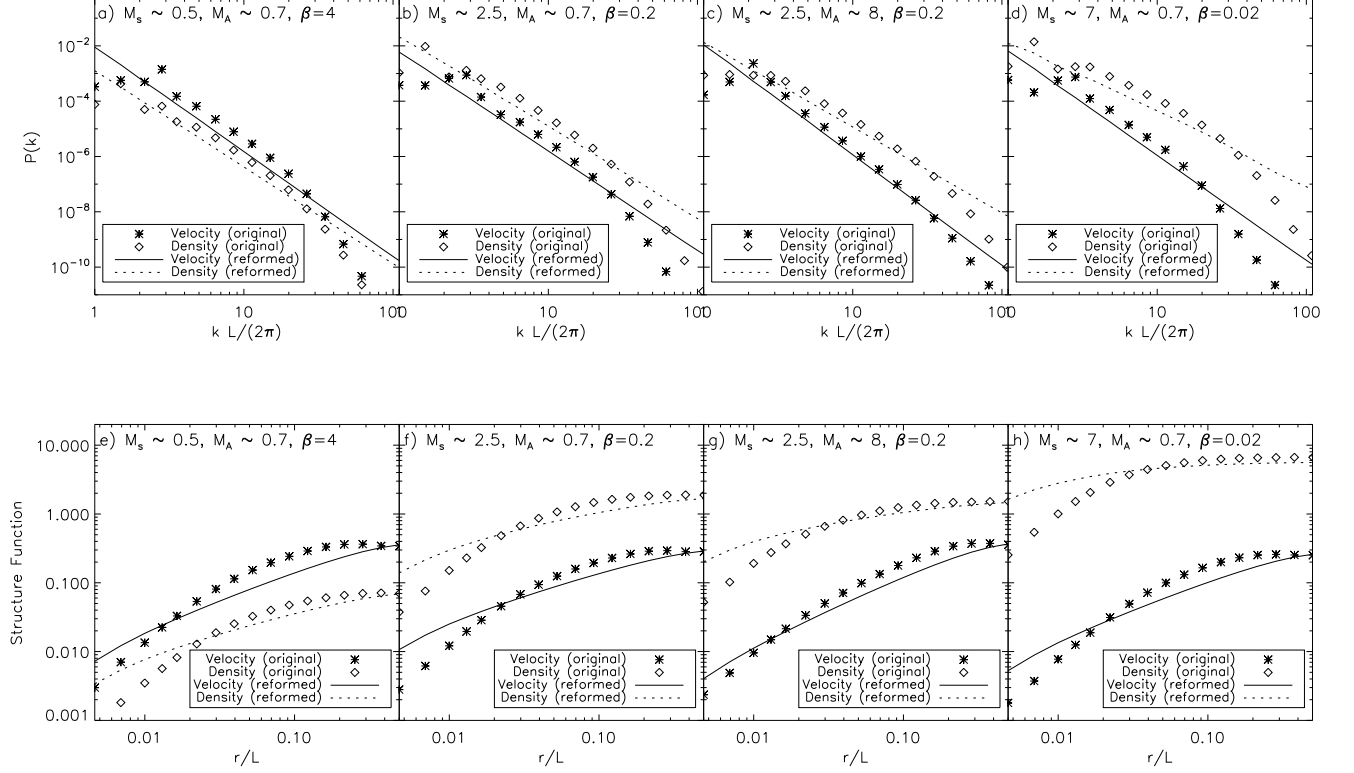


FIG. 4.— Underlying 3D statistics of the MHD simulations. At the top the power spectra, and on the bottom the corresponding structure functions. The four runs are ordered in ascendant Mach number from left to right.

4.2.2. Statistics of projected quantities (2D)

A natural way to study how the velocity centroids trace the statistics of velocity is to compare their two point statistics to those of an integrated velocity map (equation 18). This map can be used to obtain the velocity spectral index in the same way column density can be used to obtain that of density. Therefore it is a direct measure of the underlying velocity statistics (see Appendices B and C). However, it is not observable, while velocity centroids are. We computed power-spectra and structure functions of 2D maps of the various centroids (normalized, unnormalized, and “modified”), integrated velocity, and integrated density. The results for power-spectra are shown in Figures 5, and 6; for the original, and modified data-sets respectively. Similarly, Figures 7, and 8 show the results for structure functions. The most noticeable difference in the Figures is of course the larger inertial range of the reformed data-set. We also present in Table 3 a summary of spectral indices (log-log slope) measured over $5 \lesssim kL/(2\pi) \lesssim 25$ (or $1/25 \lesssim r/L \lesssim 1/5$) for the original data sets, and $kL/(2\pi) \sim [3.5 - 100]$ (or $r/L \sim [1/100 - 1/3.5]$) for the reformed sets.

Comparing the spectral indices derived in 3D (Table 2) with those of column density and integrated velocity in Table 3, one can notice a better correspondence for the reformed data-sets. This is true for the power-spectra index γ_{3D} ; as well as for m , and μ for structure functions (related by equation [16]). Directly from Figures 5–8 one can see that only for the case of subsonic turbulence (model A, $M_s \sim 0.5$) the spectrum of centroids clearly scales with that of integrated velocity. In this case the power-spectra of all the variations of centroids

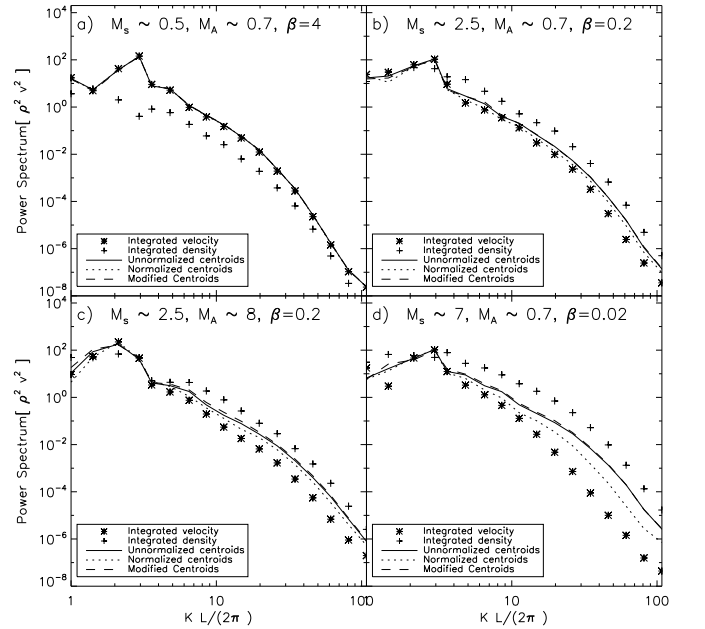


FIG. 5.— Power spectra of the integrated density (crosses), integrated velocity (stars), unnormalized, normalized, and modified centroids (solid, dotted, and dashed lines respectively) for the original set of simulations. We multiplied the spectrum of velocity fluctuations by ρ_0^2 , and that of normalized centroids by $\langle I^2 \rangle$. We show the spectrum of integrated density for reference only, to be in the same units as the other quantities in the figure it should be multiplied by v_0^2 , but since $v_0 \approx 0$ the scaling is omitted here.

TABLE 3
SPECTRAL INDICES (2D) OF QUANTITIES INTEGRATED ALONG THE LOS. THE VALUES IN PARENTHESES CORRESPOND TO THE *original* SIMULATIONS, AND IN BOLD FACE TO THE *reformed* DATA-SETS.

Model	Integrated Density		Integrated Velocity		Unnormalized Centroids		Normalized Centroids		Modified Centroids	
	$-\gamma_{3D}$	μ^*	$-\gamma_{3D}$	μ^*	$-\gamma_{3D}$	μ^*	$-\gamma_{3D}$	μ^*	$-\gamma_{3D}$	μ^*
A	(4.0) 3.5	(0.5) 1.4	(3.6) 3.8	(0.9) 1.5	(3.6) 3.8	(0.8) 1.5	(3.5) 3.8	(0.8) 1.5	(3.6) 3.7	(0.8) 1.5
B	(3.8) 3.3	(0.4) 1.2	(3.9) 3.6	(1.0) 1.4	(3.5) 3.3	(0.8) 1.1	(3.5) 3.2	(0.9) 1.1	(3.8) 3.3	(1.0) 1.0
C	(3.3) 3.1	(0.6) 1.1	(4.5) 4.0	(1.3) 1.6	(3.8) 3.4	(1.1) 1.3	(3.9) 3.5	(1.2) 1.3	(3.7) 3.4	(1.2) 1.5
D	(2.8) 2.7	(0.2) 0.7	(4.7) 3.8	(0.8) 1.5	(3.4) 2.8	(0.5) 0.9	(3.8) 2.9	(0.7) 1.0	(3.5) 2.9	(0.8) 1.1

* Since this index is not measured at scales corresponding to $R \ll z_{tot}$, but rather in the transition between the two asymptotic regimes in eq.(16), this are only lower limits on the actual μ for small lags.

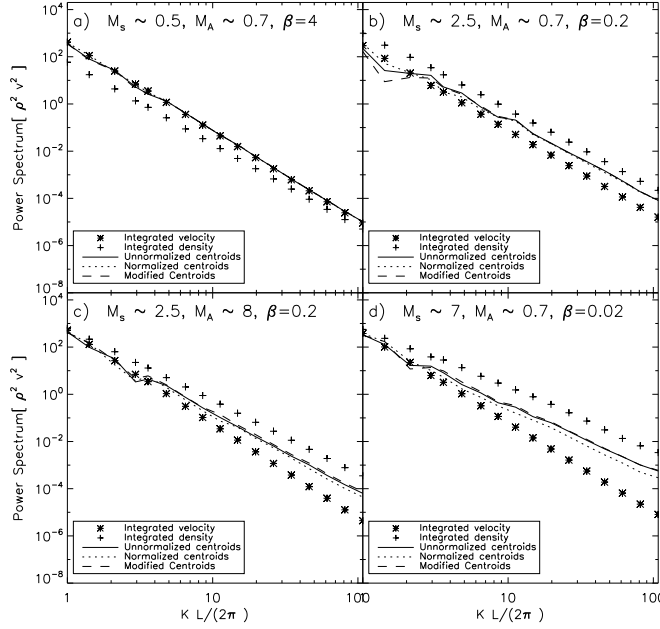


FIG. 6.— Same as Fig. 5, for the *reformed* data-sets.

recover the spectral index of velocity, within 10% error for the original simulations, and $< 3\%$ for the reformed data sets. For the cases of mildly supersonic turbulence (models B, and C, $M_s \sim 2.5$) is not clear neither from the Figures, nor from the measured slopes. While for the strongly supersonic case (model D, $M_s \sim 7$) it is obvious that velocity centroids fail to recover the velocity scaling.

Due to the finite width effects discussed at the end of §2.2, it is more difficult to determine quantitatively the spectral index from centroid maps using structure functions. According to equation (16), one should restrict to measure the spectral index for lags either much smaller, or much larger than the LOS extent of the object under study. The latter is not feasible with our simulations because the maximum lag available, unaffected by wrap-around periodicity, is $L/2 = z_{tot}/2$. The other case ($R \ll z_{tot}$) is not strictly possible with the resolution used here. For the MHD data-cubes we have to avoid the smallest scales because they are not within the inertial range (i.e. they are already dominated by dissipation). Actually, the lags used to measure μ in the original data-sets are well in the transition between the two asymptotic power-laws of equation (16). Thus, if we obtain the 3D spectral indices as

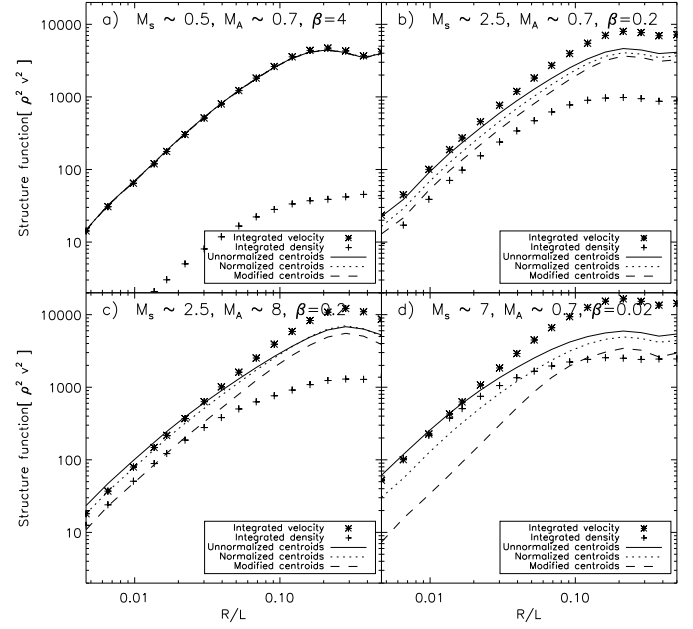


FIG. 7.— Structure functions of integrated density (*crosses*), integrated velocity (*stars*), unnormalized, normalized, and modified centroids (*solid*, *dotted*, and *dashed* lines respectively) for the *original* set of simulations. To allow for a direct comparison we scale the quantities to be all in units of $[v^2 \rho^2]$ (i. e. we multiplied the structure function of the integrated velocity by $\langle v^2 \rangle$, the integrated density by $\langle v^2 \rangle$, and the normalized centroids by $\langle I^2 \rangle$).

$\gamma_{3D} \simeq -\mu - 2$ (taking μ from Table 3), we would only get upper limits of the actual γ_{3D} . Keeping in mind that our definition of the index includes the minus sign, this means that the real index is going to be more negative than the inferred γ_{3D} from structure functions. A lower limit on the spectral index can be obtained as $\gamma_{3D} \simeq -\mu - 3$, unfortunately this provides a rather wide range of possible indices and it is not useful for practical purposes (for instance distinguishing between two models of turbulence). For the reformed data-sets the situation is better, because we can use the smallest scales. This can be verified from the better agreement of $\gamma_{3D} \simeq -\mu - 2$ with γ_{3D} measured directly from power-spectra. However, $R \ll z_{tot}$ is still not strictly fulfilled, and thus we get only lower limits of μ . We recognize this projection effect as an important drawback for the structure functions compared with spectra. Power spectra do not suffer so strongly of finite width projection effects, and could be used to obtain more accurately the spectral index of the underlying 3D index field from integrated quantities (see also Ossenkopf et al. 2005). This is true for synthetic data,

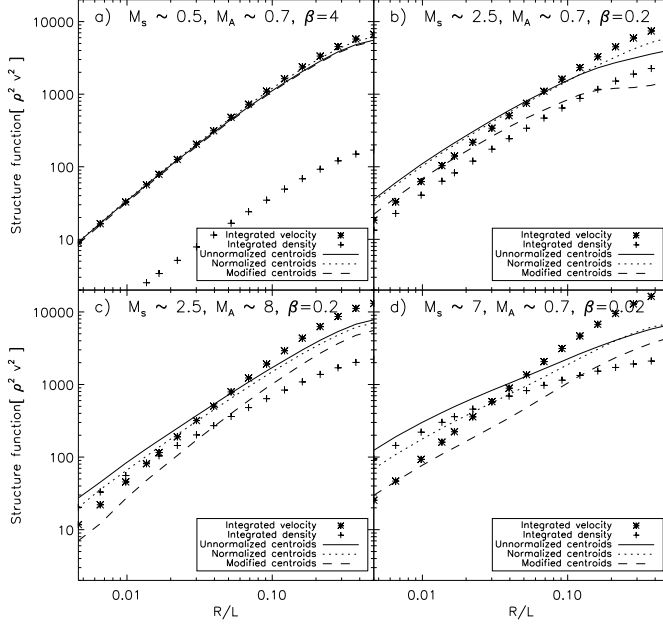


FIG. 8.— Same as Fig 7, for the *reformed* data-sets.

but for real observations power spectrum is not as reliable (see Bensch et al. 2001). At the same time, the problem of recovering quantitatively the spectral index from structure functions might be overcome for real observations with a larger inertial range. With enough spatial resolution one can have easily over two decades of inertial range in the plane of the sky (below the size of a given object along the LOS direction). In the spirit of keeping the description in terms of structure functions, which might be better suited for some type of real observations. And, using the limited range we have, it is still possible to do a comparative analysis between the spectral index of structure functions of centroids to that of integrated velocity or density.

From Figures 5–8 we see that the relative importance of the density and velocity statistics on the centroids changes with the Mach number of turbulence. For the low \mathcal{M}_s model (panels [a] in Figs. 5–8) the level of the density fluctuations is very small compared to the velocity fluctuations (weighted by $\langle v_z^2 \rangle$ and $\langle \rho^2 \rangle$ respectively) and all the centroids trace remarkably well the velocity statistics. In this case the simplified criterion $\langle \tilde{S}^2 \rangle / (\langle v_z^2 \rangle \langle \tilde{I}^2 \rangle) \gg 1$ is well satisfied: $\langle \tilde{S}^2 \rangle / (\langle v_z^2 \rangle \langle \tilde{I}^2 \rangle) \gtrsim 90$ for the original data-set, and $\gtrsim 30$ for the reformed one. This result also agrees with the notion that velocity centroids trace the statistics of velocity in the case of subsonic turbulence (where density fluctuations are expected to be negligible, as the turbulence is almost incompressible). For the rest of the models density has an increasing impact which is reflected in the centroids, and our criteria is either not entirely met, or violated. We can also see for supersonic turbulence the slope of the structure function of unnormalized centroids is almost always steeper than that of column density. This means that one needs to use the full criterion as proposed in LE03 to judge whether centroids will trace velocity or not. We will see however that our simplification of the criterion seems to discriminate when centroids trace the statistics of integrated velocity, at least for the data sets employed here. For all the supersonic cases the measured power-spectrum index from the differ-

ent centroids fail to give the index of velocity. And in general, their centroids index is found to lie between those of velocity and density, with more scatter for the original simulations compared to the reformed fields. For the original data-sets of models B, C, and D the ratio $\langle \tilde{S}^2 \rangle / (\langle v_z^2 \rangle \langle \tilde{I}^2 \rangle) \approx 5, 4, \text{ and } 3$ respectively. For the corresponding reformed data-cubes our simplified criterion gives $\langle \tilde{S}^2 \rangle / (\langle v_z^2 \rangle \langle \tilde{I}^2 \rangle) \approx 2, 4, \text{ and } 3$. In all of these cases $\langle \tilde{S}^2 \rangle / (\langle v_z^2 \rangle \langle \tilde{I}^2 \rangle) \gg 1$ is not strictly true, and indeed there is an important contribution of density fluctuations. This is consistent with the results in LE03 where we see evidence of a density dominated regime at small scales (rather density contaminated regime as centroids do not show the same index as density either). Our results agree with those presented in Brunt & Mac Low (2004), where they found that centroids do not provide good velocity representation for the supersonic turbulence they studied ($\mathcal{M}_s > 1.9$).

4.2.3. Cross-terms and density-velocity cross-correlations

The cross-terms, $I3(\mathbf{R})$, $\mathcal{F}\{B3(\mathbf{R})\}$, as well as the cross-correlations in $I4(\mathbf{R})$, and $\mathcal{F}\{B4(\mathbf{R})\}$ have contributions of velocity and density that we cannot disentangle entirely from observables. Furthermore, they cannot be expressed in terms of integrated quantities and they have to be computed from 3D statistics. We used Fourier transforms to obtain the structure, and correlation functions in 3D needed to produce independently all the terms in equations (27), and (34). These 3D statistics were integrated numerically to get $\mathcal{F}\{B3(\mathbf{R})\}$, $I3(\mathbf{R})$, $\mathcal{F}\{B4(\mathbf{R})\}$, and $I4(\mathbf{R})$. To check the accuracy of the 3D quantities obtained and our numerical integration to 2D we verified with the cases in which the statistics can be also obtained directly in 2D (e.g. $I1(\mathbf{R})$, $I2(\mathbf{R})$), finding always a good agreement. The results of the decomposition in terms of power-spectra (equation [34], after K average) are shown in Figure 9 for the original simulations, and in Figure 10 for the reformed data-sets. The decomposition for R averaged structure-functions is presented in in Figures 11, and 12; for the original, and modified data-sets respectively. Something to notice is that, because structure functions span over fewer decades in the vertical axis, the separation of all the terms is generally more clear than for power-spectra. It is also to be noticed, that for the subsonic model (A), the spectrum and structure function of centroids are almost unaffected by density fluctuations, cross-terms, or density velocity cross-correlations. Cross-correlations are found to be larger for supersonic turbulence compared to the subsonic case, but from this limited data set we can not conclude that they scale in some particular way with the sonic Mach number. It is also significant that the cross-term increases relative to the other terms with \mathcal{M}_s . For spectra, in all the supersonic models (B, C, and D) the cross-term $\mathcal{F}\{B3(\mathbf{R})\}$ is dominant. This would mean that the log-log slope measured from spectra in all of these cases is not a direct reflection of the velocity spectral index. At the same time we observe that the magnitude of density-velocity cross-correlations can only be entirely ignored for model A (subsonic turbulence). For structure functions the cross-term is comparable or larger in magnitude than the contribution of column density. At the same time it gets closer, but does not become larger than $I2(\mathbf{R})$. In fact, it was found to be always steeper than the velocity term, therefore its contribution at the small scales could be neglected. Velocity-density cross-correlations in $I4(\mathbf{R})$ for all the cases we con-

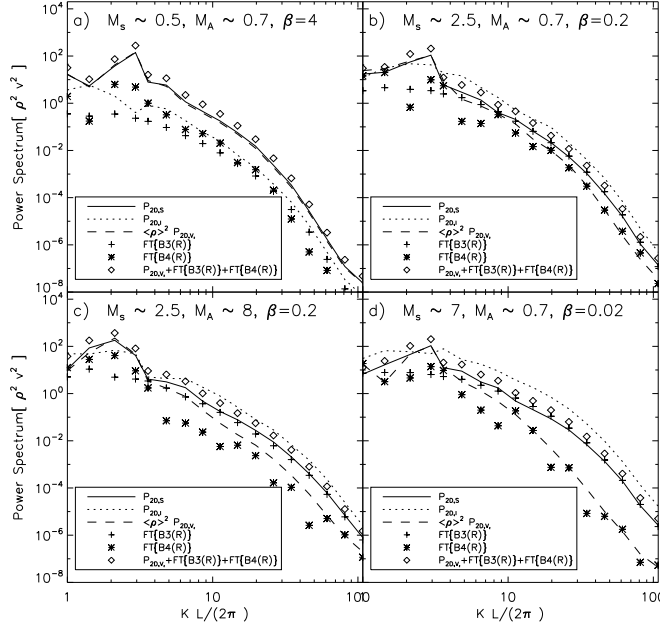


FIG. 9.— Decomposition of the spectra of unnormalized velocity centroids as in equation 34 (with $v_0 \approx 0$), for the *original* data-sets. The *solid* line is the spectrum of the 2D map of velocity centroids. The *dotted* line (for reference only) is the power spectrum of column density, the *dashed* is the spectrum of integrated velocity, both obtained from integrated (2D) maps. The *crosses* represent the cross-term $\mathcal{F}\{B3(\mathbf{R})\}$, and the “X” correspond to density-velocity cross-correlations $\mathcal{F}\{B4(\mathbf{R})\}$. This last two were computed from 3D statistics, then integrated along the LOS. The *diamonds* show the sum of all the terms in the decomposition to compare with the *solid* line.

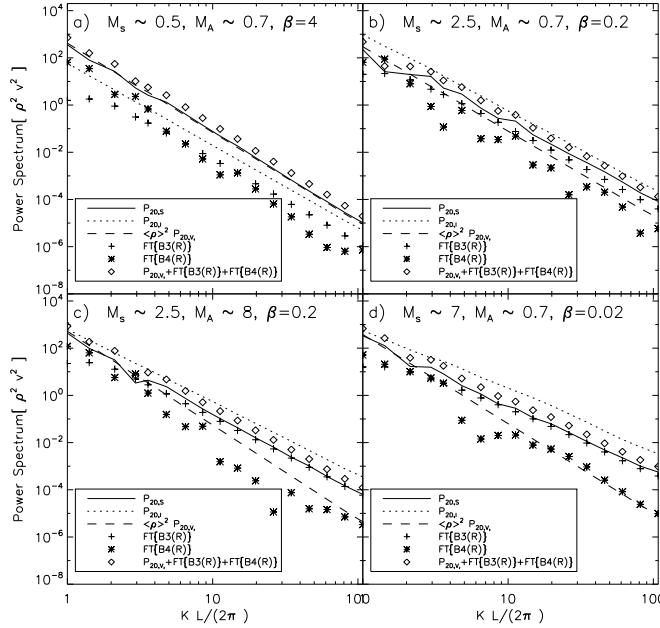


FIG. 10.— Same as Fig. 9, for the *reformed* data-sets.

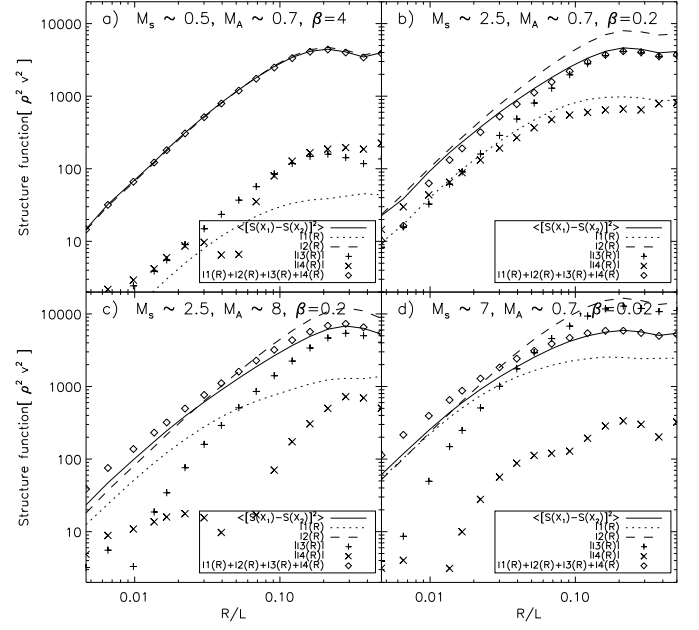


FIG. 11.— Decomposition of the structure function of unnormalized velocity centroids (eq.[27]), for the *original* data-sets. The *solid* line is the structure function of the 2D map of velocity centroids. The *dotted* line is $I1(\mathbf{R})$, the *dashed* $I2(\mathbf{R})$, both obtained from 2D maps. The cross-term $I3(\mathbf{R})$ as *crosses*, while the density-velocity cross-correlations ($I4(\mathbf{R})$) are the “X”. This last two were computed from 3D statistics, then integrated along the LOS. The *diamonds* show the sum of all the terms in the decomposition to compare with the *solid* line.

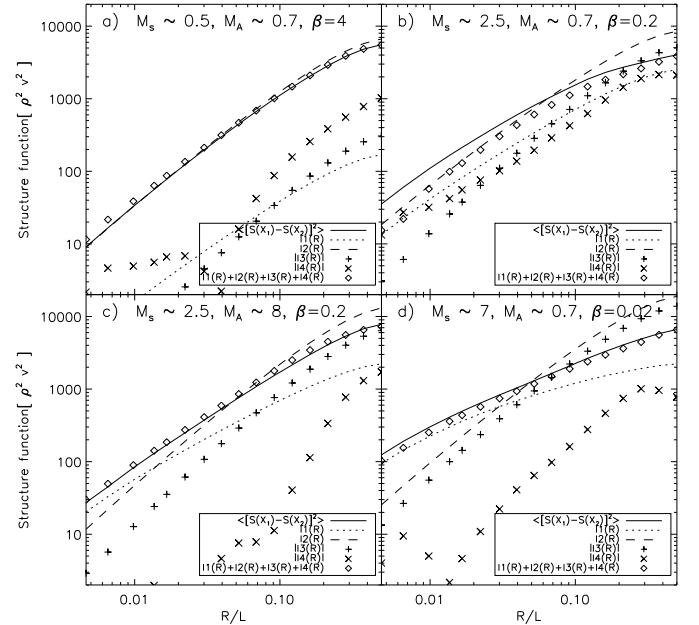


FIG. 12.— Same as 11, for the *reformed* data-sets.

sidered here⁵ never had an important impact on the statistics of centroids. Anyway, $I3(\mathbf{R}) + I4(\mathbf{R})$ as a whole (especially at the smallest separations, which we are most interested in)

⁵ The situations when velocity-density correlations are dominant are discussed in our next paper

has been found to be smaller than the integrated velocity term. Suggesting that there could be cases where $I3(\mathbf{R}) + I4(\mathbf{R})$ – the cross-term and cross-correlations – can be neglected. However, since the indices from power-spectra of centroids failed to give the velocity spectral index for models B, C, and D, we conclude that the retrieval of spectral indices from velocity centroids over the entire inertial range should be restricted to very low sonic Mach numbers ($M_s < 2.5$). Furthermore, the relative importance of the cross-terms grow together with the column density term as the strength of turbulence increases. For $M_s \sim 7$ certainly the contribution of the column density is considerable. In this case MVCs could be used to remove the contribution from the column density term in the structure function of centroids. However at such high Mach number the cross-terms cannot be neglected either.

At a first glance it might seem surprising that the velocity centroids could be dominated by velocity even when the 3D structure functions of density had a zero point (offset) larger than that of velocity. This effect arises primarily from the fact that the density is positive defined, and necessarily has a non zero mean whereas the velocity field can have a zero mean. This results in the factors that multiply the density and velocity structure functions in equation (24). The factor $\langle v_z^2 \rangle = v_0^2 + \langle \tilde{v}_z^2 \rangle$ multiplies the density structure function, and we can minimize the undesired density contribution by shifting our velocity axis in such a way that $v_0 = 0$. For a more detailed discussion about the velocity and density zero levels see Ossenkopf et al. (2005).

5. VELOCITY CENTROIDS AND ANISOTROPY STUDIES IN SUPERSONIC TURBULENCE

We have seen how density fluctuations in supersonic turbulence affect our ability to determine the velocity spectral index from observations. But is there something else velocity centroids could be used for, even in supersonic turbulence? The presence of a magnetic field introduces a preferential direction of motion, thus breaking the isotropy in the turbulent cascade. In a turbulent magnetized plasma, eddies become elongated along the direction of the *local* magnetic field. Velocity statistics have been suggested to study this anisotropy (Lazarian et al. 2002; Esquivel et al. 2003; Vestuto et al. 2003)⁶. For instance, iso-contours of two point statistics of velocity centroids instead of being circular, as in the isotropic case, are ellipses with symmetry axis that reveals the direction of the *mean* magnetic field. We present in Figure 13 contours of equal correlation of velocity centroids (unnormalized) from our simulations. The magnitude of the magnetic field determines how much anisotropy will be present. We can see from Figure 13 that the anisotropy is very clear for models A, B, and D, regardless of the large differences in sonic Mach number and plasma β . The only case in which the anisotropy is not evident (model C) is our only super-Alfvénic simulation. The concept of super-Alfvénic turbulence is advocated, for instance, by Padoan et al. (2004b) for molecular clouds.

Another way to visualize the anisotropy is to plot the correlation functions of centroids in the parallel or perpendicular directions relative to B_0 , this is shown in Figure 14. In our simulations this corresponds to plot the value at the intercepts in Figure 13, in observations it would mean to plot

⁶ Both velocity centroids and spectral correlation functions were demonstrated to trace the magnetic field in Lazarian et al. (2002), channel maps were studied for the same purpose in Esquivel et al. (2003), and velocity centroids in Vestuto et al. (2003)

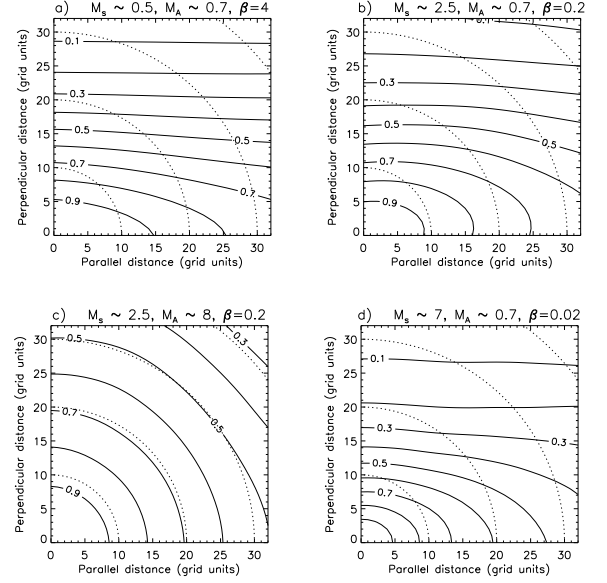


FIG. 13.— Anisotropy in the correlation functions: contours of equal correlation for the simulations (solid lines). For reference we show isotropic contours as dotted lines. The sonic and Alfvén Mach numbers (M_s , M_A respectively) are indicated in the title of the plots. The anisotropy reveals the direction of the magnetic field for all the sub-Alfvénic cases, regardless of the sonic Mach number.

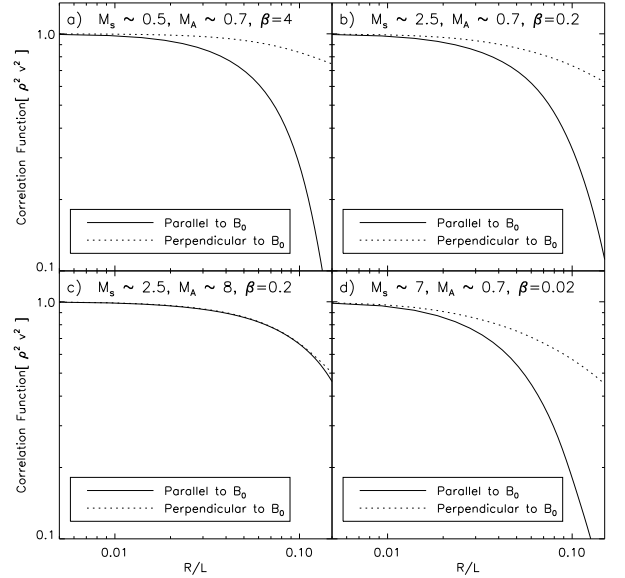


FIG. 14.— Correlation functions taken in directions parallel and perpendicular to the mean magnetic field. The anisotropy shows in the different scale-lengths for the distinct directions. It is noticeable the little difference in panels (a), (b), and (d). Which correspond to the same ratio \tilde{B}/B_0 , but very different sonic Mach numbers. Panel (c) corresponds to super-Alfvénic ($\tilde{B} > B_0$) turbulence, and the anisotropy is not evident in the centroid maps.

the correlation function only along the major or minor axis of the contours of equal correlation. the anisotropy is evident as a different scale-length (correlation-length) for correlations in the parallel or perpendicular to the mean magnetic field. For subsonic turbulence the degree of anisotropy reflects the ratio $(\tilde{B}/B_0)^2$. However for supersonic turbulence as the contributions of density get important, and as density at high Mach number gets more isotropic (see Beresnyak et al.

2005), one could expect the anisotropy to decrease while the ratio \tilde{B}/B_0 stays the same. We found very little evidence of this decrease, as can be verified from models A, B, and D in Figure 14, all the three runs have the same \tilde{B}/B_0 , and a large contrast in sonic Mach number. In model C even though the magnetic pressure is larger than the gas pressure ($\beta = 0.2$), it corresponds to a weak mean field $\tilde{B} > B_0$. In this case the magnetic field has very chaotic structure at large scales (see Cho & Lazarian 2003). As the fluctuations at large scale determine the anisotropy of the projected data, the MHD anisotropy is erased after LOS averaging.

Whether the ISM is sub-Alfvénic is still up for debate. The fact that centroids are only anisotropic for sub-Alfvénic turbulence gives us an opportunity to study the conditions under which that is the case. It is certainly encouraging, that for sub-Alfvénic turbulence the degree of anisotropy does not seem to be strongly affected by density fluctuations. However, we should add a word of warning in trying to determine the ratio \tilde{B}/B_0 from velocity centroids in supersonic turbulence. The fact that centroids do not represent velocity for $\mathcal{M}_s > 2.5$ calls for some caution as to what extent the ratio \tilde{B}/B_0 can be obtained from observations. Nonetheless, the result on the direction of the mean field is rather robust, including for highly supersonic turbulence, provided a relatively large ordered component B_0 . Anisotropies of turbulence measured by different techniques, including centroids, provide a promising way of measuring the direction of the perpendicular to the LOS component of the magnetic field. For practical purposes the technique can be tested using polarized radiation arising from aligned dust grains (see Lazarian 2003 for a discussion of grain alignment), or CO polarization arising from Goldreich-Kylatis effect (see Lai, Girart & Crutcher 2003).

For any particular observational data one should bear in mind that only the plane-of-sky components of mean and fluctuating magnetic field are available. Therefore, for instance, a cloud with sub-Alfvénic turbulence but with a mean magnetic field directed along the line of sight would look like a cloud with super-Alfvénic turbulence. The distinction between the two cases may be done, however, using an ensemble of clouds. It is unlikely to have mean magnetic field always directed towards the observer. If, indeed, the turbulence is typically sub-Alfvénic, the anisotropy should show up in centroid maps.

6. DISCUSSION

We used MHD data-cubes to produce centroid maps, and explored the limitations of velocity centroids for studying interstellar turbulence.

We investigated numerically the analytical predictions in our previous study of velocity centroids (LE03). In that work, we decomposed the structure function of velocity centroids into three main contributions, namely integrated (or column) density, integrated velocity, and “cross-terms”. By calculating separately all the terms in the structure function of unnormalized centroids we showed that the decomposition works well.

We found two important restrictions on the procedure accuracy, both related to the finite resolution in the numerical simulations. First, structure functions of integrated quantities can in principle be used to retrieve the underlying 3D spectral index if calculated for lags either much greater or much smaller than the LOS extent of the object. We showed however, that with the resolution used here (216^3) structure function of integrated quantities can only give an upper limit on the actual

spectral index. Second, the limited inertial range in our simulations present an additional constraint on the accuracy of estimating the spectral index, mainly because the measured log-log slope is very sensitive the range of scales used.

In regards to the finite width projection effects one can potentially still do a comparative study of the centroid statistics with the statistics of velocity and density. That is, we can compare the spectral index of the centroid maps to that of column density or integrated density, and see to which one is closer. However, for real observational data with the possibility to sample lags $R \ll z_{tot}$, obtaining the 3D spectral index directly from structure functions is not a problem.

Power-spectrum is an alternative to obtain the scaling properties of the turbulent velocity field that does not suffer of such projection effects (i.e. the spectral index can be measured at any wave-numbers within the inertial range). In order to use power-spectra too, we constructed a power-spectra decomposition analogous to that in LE03. And, by calculating each term separately, we tested successfully the validity of this decomposition.

We found that the scaling properties of the underlying velocity field (i.e. spectral index) can be reliably retrieved for subsonic turbulence. However, the contamination from cross-terms clearly showed up in all the supersonic cases for spectra, while for structure functions it was only evident for $\mathcal{M}_s \sim 7$. To alleviate the other problem (not enough inertial range) we introduced reformed versions of the original simulations. The power spectra of new data-set are strict power-laws, with almost the same spatial structure, and density-velocity cross-correlations. The spectral indices obtained with these reformed data sets are in better agreement with the analytical predictions.

We also tested successfully a criterion for which velocity centroids give trustworthy information (equation [35]), that can be obtained entirely from observations. For practical purposes we suggest as the first approach an approximation of the criterion in LE03 in terms only of the variances of the maps of column density and velocity centroids instead of computing all the structure function (equation [36]). If this ratio is less than unity velocity centroids are not trustworthy. When the ratio in eq.(36) is small but larger than unity it is recommendable to use the full criterion, as proposed in LE03. In our only case of subsonic turbulence (model A) centroids traced the integrated velocity structure function extremely well. And, our simplified criteria was fulfilled: $\langle \tilde{S}^2 \rangle / (\langle v_z^2 \rangle \langle \tilde{I}^2 \rangle) \gtrsim 90, 30$, for the original, and reformed data-set respectively. For the rest of the models (B, C, D) the criteria was not satisfied ($\langle \tilde{S}^2 \rangle / (\langle v_z^2 \rangle \langle \tilde{I}^2 \rangle) \gtrsim [5-2]$), and the centroids failed to trace the statistics of the velocity field. In this models one can see a better correspondence between centroids and integrated velocity for the $\mathcal{M}_s \sim 2.5$ runs compared to the highly supersonic case $\mathcal{M}_s \sim 7$. Thus, one might hope centroids to be able to trace the spectral index of velocity for supersonic turbulence, but only for $\mathcal{M}_s < 2.5$. We must recognize that this study was done using a limited data set. A more complete exploration of parameter space is desirable to determine better the range of applicability of velocity centroids, including MVCs.

We have seen that velocity centroids are only reliable at low Mach numbers. At the same time there are other techniques available that work for strongly supersonic turbulence, such as VCA and VCS. The techniques are complementary and can be used simultaneously. For subsonic turbulence, VCA and VCS can be used with higher mass species. Note, that the differ-

ent techniques pick up different components of velocity tensor. This can potentially allow a separation of compressional and solenoidal parts of the velocity field (LE03). Determining these components are crucial for understanding properties of interstellar turbulence, its sources and its dissipation.

We stress that every technique has its own advantages. Velocity centroids can reproduce velocity better than VCA and VCS when the velocity statistics is not a straight power-law. Therefore velocity centroids can better pick up dissipation and injection of energy scales.

Nonetheless, one have to bear in mind that spectral indices derived from all of the techniques above do not provide a complete description of turbulence. Anisotropy is another parameter that can be studied. For instance, we showed that velocity centroids are useful to study the anisotropy of the turbulent cascade, even for highly supersonic turbulence. We showed however, that this is restricted to a relatively large mean field. For super-Alfvénic turbulence, a model favored by some researchers (Padoan et al. 2004a), the anisotropy of centroids is marginal, which allows to test these theories. Anisotropy is not only present in velocity centroid maps, but in other statistics as well, such as *spectral correlation function* (see Lazarian et al. 2002). Combining the two measure can improve the confidence in the results.

Additionally, we need tools to study the turbulence variations in space (i.e. intermittency). Higher order velocity structure functions (those described in this paper are second order) have been shown to be a promising for such studies (see Müller & Biskamp 2000; Cho et al. 2003). Velocity centroids can be easily recasted in terms of higher order statistics, opening a new window for intermittency studies. Is worth noting that higher moments can provide the directions of the intermittent structures if those get oriented in respect to magnetic field. Our results indicate that such studies can be carried out even for high Mach number turbulence. In addition, studies of intermittency with centroids can be incorporated to other techniques. For instance, the interpretation of results of the Principal Component Analysis (PCA) technique suggested as a tool for turbulence studies by Heyer & Schloerb (1997) depends on the degree of intermittency of turbulence (Brunt et al. 2003; Heyer 2004 private communication).

Velocity centroids have been used for studies of turbulence for many decades. How can we comment on these studies from the point of view of our present theoretical understanding? Let us glance at the available studies. Turbulence in H II regions is usually subsonic. Therefore velocity centroids could be probably trustworthy there (see O'Dell & Castaneda 1987). Supersonic turbulence in molecular clouds (see Miesch & Bally 1994) is a field where velocity centroids might be in error. The same is probably true for H I studies (see Miville-Deschênes et al. 2003a)⁷ where turbulence is highly supersonic in cold H I.

We feel that a more careful analysis of particular conditions present in the regions under study is necessary, however. One one hand, while the turbulence is supersonic for molecular clouds, the cores of molecular clouds are mostly subsonic (see Tafalla et al. 2004; Myers & Lazarian 1998). For such cores velocity centroids provide a reliable tool for obtaining velocity statistics, if the resolution of the cores is adequate. On the

other hand, our results are based on the analysis of isothermal numerical simulations. In the presence of substantial density contrasts caused by the co-existence of different phases the velocity centroids may get unreliable even for subsonic turbulence. Therefore testing of the necessary criteria discussed in this paper may be advantageous not only with the molecular and H I data, but also with data obtained for H II regions. We also note, that for the present analysis we assumed that the emission is optically thin and the emissivity is proportional to the first power of density. Discussion of more complex, but still observationally valuable cases will be done elsewhere. The work started in this direction (see Lazarian & Pogosyan 2004) is encouraging.

Recent work on centroids includes papers by Ossenkopf & Mac Low (2002) where they noticed that centroids poorly reproduce velocity statistics for supersonic turbulence. Our work above confirms their finding and also establishes a regime ($\mathcal{M}_s < 2.5$) when the results by centroids can be reliable.

A quite different and optimistic conclusion about centroids was obtained in Miville-Deschênes et al. (2003b). They used Brownian noise artificial data and obtained an excellent correspondence between the centroids and the underlying velocity. From the point of view of our analysis the origin of this correspondence is in the choice of the mean density level. In these simulation in order to make the density positively defined the authors were adding a substantial mean density to the fluctuating density. It is clear from eq.(29) that adding mean density increases of the contribution of $I2(\mathbf{R})$ term that is the term responsible for the velocity contribution.

This work is complementary to the work on delta variance of centroids that we do in collaboration with Ossenkopf & Stutzki (Ossenkopf et al. 2005). There Brownian noise simulations are used, but extra care is taken to avoid being misled by the effect of adding mean density. An iterative procedure is proposed there, which allows to correct for the contribution of the cross-terms when density-velocity correlations are negligible.

In this paper we are dealing mostly with unnormalized centroids. The modified centroids (MVCs) allow a different outlook at the problem of obtaining velocity statistics from the small scale asymptotics. Indeed, our analysis in the paper shows that the term $I4(\mathbf{R})$ is unimportant for the cases that we studied. In addition, we believe that velocity has steep spectra. Therefore, if the density is also steep, asymptotically the term $I3(\mathbf{R})$, which is then steeper than both velocity and density, should be negligible (see Appendix E.1). As the result, *if we see from the integrated intensity maps that density indeed is steep, we can use MVCs as suggested in LE03*, that for sufficiently small lags are bound to represent the velocity statistics. The critical scale at which this is true can be obtained using the analytical expressions found in Appendix B.1. Formally to find such critical scale one should know the mean density. However, if the inertial range is sufficiently long, one should not be worried about the exact value for that critical scale.

We have not seen much advantages of such a use in our numerical runs because of the limited inertial range available. However, unlike numerical simulations, astrophysical conditions provide us with a substantially larger inertial range. For instance, Stanimirović & Lazarian (2001) showed that the turbulent spectrum for velocity spans from the size of the SMC, which is ~ 4 kpc, to the minimal scale resolved, i.e. ~ 40 pc. In partially ionized gas we expect this spectrum to proceed to sub-parsec scales. In fully ionized gas (see also discussion

⁷ An interesting feature found in Miville-Deschênes et al. (see 2003a) is that the statistics of velocity centroids is almost identical to the statistics of density field. This could be due to the dominance of the $I1$ term, which can be tested.

in Lazarian et al. 2004) the scale of Alfvén and slow mode damping may be hundreds of kilometers only.

The limitations of this asymptotic approach stem from the fact that for supersonic turbulence the density field tends to become shallower. But, as we can see from the MHD simulations used here, at $\mathcal{M}_s \sim 2.5$ we find that it is still steep and therefore the MVCs should be reliable asymptotically. Therefore, for handling observational data we can provide another prescription: “If the inertial range is sufficiently long and density is steep then MVCs asymptotically represent the velocity field.” For instance, steep density was reported in Miville-Deschênes et al. (2003b). Thus for such density fields asymptotic use of MVCs should be advantageous.

In the cases when the underlying statistics is not a power law the interpretation of centroids is more involved. This we have seen with our analysis of non-power-law data from MHD simulations. While centroids do represent injection and damping scales, the integration along the line of sight does interfere with a more fine detail study. In this situations one should use the full technique of inversion as proposed in Lazarian (1995). However, we expect that in most cases astrophysical turbulence is self-similar over large expanses of scales and therefore the power-law representation is adequate.

We have made use of the analytical expressions for unnormalized velocity centroids (LE03). Our work as well as a study in Levrier (2004), show that normalization of centroids improve them rather marginally, while it makes the analytical insight essentially impossible. In this paper we tested that major conclusions reached for unnormalized centroids are applicable to the normalized ones.

7. SUMMARY

In this paper we have provided a systematic study of velocity centroids as a technique of retrieving velocity statistics from observations. We used both results of MHD simulations as well as “reformed” data-sets which have larger inertial range. We found:

1. Centroids of velocity can be successfully used to retrieve the scaling properties of the underlying 3D velocity field for subsonic turbulence. For supersonic turbulence with sonic Mach number $\gtrsim 2.5$ velocity centroids failed to trace the spectral index of velocity.
2. Our numerics confirmed the expression for centroid statistics obtained in LE03. And, in particular, we tested successfully the criterion in LE03 for the reliable use of velocity centroids. We showed that it reflects a

necessary condition for centroids to reproduce the velocity statistics.

3. We studied modified velocity centroids (MVCs) proposed in LE03. It is shown that MVCs reflect the statistics of velocity better than unnormalized centroids for small lags. This result is valid for both steep and shallow density fields with steep velocity.
4. We showed that velocity-density cross-correlations are marginally important for our data set, at least for small lags. Combined with the fact that products of density and velocity structure functions get subdominant for steep velocity and density at small lags, this provides a way to reliably study turbulence using MVCs.
5. We demonstrated that velocity centroids can be used for both subsonic and supersonic turbulence to study the anisotropy introduced by the magnetic field. Even when they fail to retrieve the velocity spectral index in supersonic turbulence. For up to at least $\mathcal{M}_s \sim 7$ they for sub-Alfvénic turbulence provide reliably the direction of the component of the magnetic field perpendicular to the LOS.
6. If turbulence is super-Alfvénic it results in a marginal anisotropy of velocity centroids which provides a good way to test whether the Alfvén Max number of turbulence in molecular clouds is less or larger than unity.
7. Within their domain of applicability, centroids of velocity provide a good tool for turbulence studies that should be used in conjunction with other tools, e.g. VCA and VCS.

We thank Jungyeon Cho for supplying us with the data cubes of MHD turbulence simulations, Anthony Minter, the referee of LE03, as well as the anonymous referee of this paper, for suggestions that benefited this work. We would like to thank especially V. Ossenkopf and J. Stutzki for many insightful discussions, in fact great part of the improvements of the manuscript have been made in collaboration with them. A. E. acknowledges financial support from CONACYT (Mexico). A. L. research is supported by NSF grant AST 0307869 and the NSF Center for Magnetic Self Organization in Laboratory and Astrophysical Plasmas.

APPENDIX

A. TURBULENCE STATISTICS IN THREE DIMENSIONS

A.1. Turbulence statistics in real (xyz) space.

The two-point correlation function of a vector field $\mathbf{u}(\mathbf{x}) = [u_x(\mathbf{x}), u_y(\mathbf{x}), u_z(\mathbf{x})]$ is defined as:

$$B_{ij}(\mathbf{r}) \equiv \langle u_i(\mathbf{x}_1) u_j(\mathbf{x}_2) \rangle, \quad (\text{A1})$$

where $\mathbf{r} = \mathbf{x}_2 - \mathbf{x}_1$ is the separation or “lag”, in Cartesian coordinates $i, j = x, y, z$, and $\langle \dots \rangle$ denote ensemble average over all space. An additional definition can be made in terms of the fluctuations of the field. This can be obtained formally by replacing $\mathbf{u}(\mathbf{r})$ by $\tilde{\mathbf{u}}(\mathbf{x}) = \mathbf{u}(\mathbf{x}) - \langle \mathbf{u}(\mathbf{x}) \rangle$ in equation (A1). Note that this necessarily implies $\langle \tilde{\mathbf{u}} \rangle = 0$. We will refer to this variation simply as correlation function of fluctuations, and denote it by

$$\tilde{B}_{ij}(\mathbf{r}) \equiv \langle \tilde{u}_i(\mathbf{x}_1) \tilde{u}_j(\mathbf{x}_2) \rangle = B_{ij}(\mathbf{r}) - \langle u_i \rangle \langle u_j \rangle. \quad (\text{A2})$$

In the same manner, it is customary to define the structure function of the same vector field $\mathbf{u}(\mathbf{x})$ as

$$\begin{aligned} D_{ij}(\mathbf{r}) &\equiv \langle [u_i(\mathbf{x}_1) - u_i(\mathbf{x}_2)] [u_j(\mathbf{x}_1) - u_j(\mathbf{x}_2)] \rangle \\ &= \langle [\tilde{u}_i(\mathbf{x}_1) - \tilde{u}_i(\mathbf{x}_2)] [\tilde{u}_j(\mathbf{x}_1) - \tilde{u}_j(\mathbf{x}_2)] \rangle. \end{aligned} \quad (\text{A3})$$

Notice that structure functions, by definition, depend only on the fluctuating part of the field and are insensitive to the mean value of the field. Combining equations (A1) and (A3) it is trivial that:

$$D_{ij}(\mathbf{r}) = 2 [\tilde{B}_{ij}(0) - \tilde{B}_{ij}(\mathbf{r})] = 2 [B_{ij}(0) - B_{ij}(\mathbf{r})]. \quad (\text{A4})$$

Where $\tilde{B}_{ij}(0)$ is also known as the variance. The correlation of fluctuations must vanish at infinity, that is $\tilde{B}_{ij}(\mathbf{r}) \rightarrow 0$, as $r \rightarrow \infty$. Then from equation (A4) is clear that $D_{ij}(\infty) = 2\tilde{B}_{ij}(0)$. Thus, if we know the structure function of a field we can obtain the correlation function of fluctuations and vice versa. However, to get the correlation function in general (as in equation [A1]) we also need to know the mean value of the field ($\langle \mathbf{u} \rangle$). Correlation and structure functions are equivalent in theory. In practice however, where we have a restricted averaging space, it is easier to determine $D_{ij}(\mathbf{r})$ more accurately compared to $B_{ij}(\mathbf{r})$. At the same time, $\tilde{B}_{ij}(0)$ is usually better determined than $D_{ij}[\infty]$ (see discussion in Monin & Yaglom 1975).

Alternatively, we can use spectral representation to describe turbulence. The *spectral density tensor*, or *N-dimensional power-spectrum*, $F_{ij}(\mathbf{k}) = P_{ND}(\mathbf{k})$, is given through a Fourier transform of the correlation function of fluctuations:

$$F_{ij}(\mathbf{k}) = P_{ND}(\mathbf{k}) \equiv \frac{1}{(2\pi)^N} \int e^{-i\mathbf{k} \cdot \mathbf{r}} \tilde{B}_{ij}(\mathbf{r}) d^N \mathbf{r}, \quad (\text{A5})$$

where \mathbf{k} is wave-number-vector. The definitions presented above are general, and also apply to scalar fields.

The power-spectrum of velocity (in the incompressible regime) has an important physical interpretation as the distribution of kinetic energy (per unit mass) as a function of scale. If $\mathbf{u}(\mathbf{r})$ is the velocity field, the power-spectrum is the energy in scales between \mathbf{k} and $\mathbf{k} + \delta\mathbf{k}$, and thus the total energy is proportional to $\langle \mathbf{u}(\mathbf{r})^2 \rangle = \int P_{ND}(\mathbf{k}) d\mathbf{k}$. Note however, that the physical interpretation is quite different if we talk about the spectra of other quantity (e.g. the power-spectra of density fluctuations). For isotropic fields the correlation, structure or spectral tensors can be expressed via longitudinal (parallel to \mathbf{r} , denoted by subscript “LL”) or transverse (normal to \mathbf{r} , denoted by subscript “NN”) components (Monin & Yaglom 1975):

$$B_{ij}(r) = [B_{LL}(r) - B_{NN}(r)] \frac{r_i r_j}{r^2} + B_{NN}(r) \delta_{ij}, \quad (\text{A6})$$

$$D_{ij}(r) = [D_{LL}(r) - D_{NN}(r)] \frac{r_i r_j}{r^2} + D_{NN}(r) \delta_{ij}, \quad (\text{A7})$$

$$F_{ij}(k) = [F_{LL}(k) - F_{NN}(k)] \frac{k_i k_j}{k^2} + F_{NN}(k) \delta_{ij}, \quad (\text{A8})$$

where δ_{ij} is a Kronecker delta ($\delta_{ij} = 1$ for $i = j$, and $\delta_{ij} = 0$ for $i \neq j$). Solenoidal motions (divergence free, therefore incompressible) correspond to the transverse components whereas potential motions (curl free, compressible) correspond to the longitudinal components.

A.2. Turbulence statistics as observed (position-position-velocity space)

Spectroscopic observations do not provide the distribution of gas in real space coordinates ($\mathbf{x} \equiv [x, y, z]$). Instead we observe the intensity of emission of a given spectral line at a position \mathbf{X} in the sky, and at a given velocity v along the LOS (we use capital letters for 2D vectors and lower case for 3D vectors). Observational data are usually arranged in matrices with coordinates (\mathbf{X}, v) , also called position-position-velocity (or simply PPV) cubes. We will identify the LOS with the coordinate z . Thus, in the plane parallel approximation the relation between real space and PPV space is that of a map $(\mathbf{X}, z) \rightarrow (\mathbf{X}, v_z)$, with $\mathbf{X} = (x, y)$.

At any point the LOS velocity can be decomposed in a regular flow, a thermal, and a turbulent components [$v_z(\mathbf{x}) = v_{z,reg}(\mathbf{x}) + v_{thermal} + v_{z,turb}(\mathbf{x})$]. This way, the distribution of the Doppler shifted atoms follows is a Maxwellian of the form:

$$\phi(\mathbf{x}) dv_z = \frac{1}{(2\pi\beta)^{1/2}} \exp \left\{ -\frac{[v_z - v_{z,reg}(\mathbf{x}) - v_{turb,z}(\mathbf{x})]^2}{2\beta} \right\} dv_z, \quad (\text{A9})$$

where $\beta = \kappa_B T / m$, κ_B is the Maxwell-Boltzmann constant, T the temperature, and m the atomic mass. In PPV space, the density of emitters $\rho_s(\mathbf{X}, v_z)$ can be obtained integrating along the LOS

$$\rho_s(\mathbf{X}, v_z) d\mathbf{X} dv_z = \left[\int dz \rho(\mathbf{x}) \phi(\mathbf{x}) \right] d\mathbf{X} dv_z, \quad (\text{A10})$$

where $\rho(\mathbf{x})$ is the mass density of the gas in spatial coordinates. The density of emitters $\rho_s(\mathbf{X}, v_z)$ can be identified as the column density per velocity interval, commonly referred as dN/dv . Equation (A10) simply counts the number of atoms at a position in the plane of the sky \mathbf{X} , with a z component of velocity in the range $[v_z, v_z + dv_z]$, and the limits of integration are defined by the LOS extent. The integrated intensity of the emission (integrated along the velocity coordinate) corresponds to the column density under the assumptions of optically thin media and emissivity linearly proportional to the density:

$$I(\mathbf{X}) \equiv \int \alpha \rho_s(\mathbf{X}, v_z) dv_z = \int \alpha \rho(\mathbf{x}) dz. \quad (\text{A11})$$

B. PROJECTION OF STRUCTURE FUNCTIONS OF A POWER-LAW SPECTRUM FIELD

In this section we exemplify the long-wave dominated (steep) case as if coming from a velocity field, while the shallow case as if from a density field. The results are interchangeable, depending on the specific spectral index they have (although there is no physical motivation to consider a shallow the velocity field).

B.1. Projection of a field with a steep power spectrum

Consider a homogeneous, and isotropic velocity field with a *steep* power-law spectrum. The LOS (chosen to correspond with the z direction) velocity structure function will be of the form:

$$\langle [v_z(\mathbf{x}_1) - v_z(\mathbf{x}_2)]^2 \rangle = C_1 r^m. \quad (\text{B1})$$

Where $r = \sqrt{R^2 + (z_2 - z_1)^2}$, R is the separation in the plane of the sky ($R^2 = [x_2 - x_1]^2 + [y_2 - y_1]^2$), and $(z_2 - z_1)$, the separation along the LOS. This way we can rewrite the 3D power-law structure function as

$$\langle [v_z(\mathbf{x}_1) - v_z(\mathbf{x}_2)]^2 \rangle = C_1 [R^2 + (z_2 - z_1)^2]^{m/2}. \quad (\text{B2})$$

The projection of the velocity field, as described in §§2.2 results in

$$\langle [V_z(\mathbf{X}_1) - V_z(\mathbf{X}_2)]^2 \rangle = C_1 \int_0^{z_{tot}} \int_0^{z_{tot}} \left\{ [R^2 + (z_2 - z_1)^2]^{m/2} - (z_2 - z_1)^m \right\} dz_2 dz_1. \quad (\text{B3})$$

Where z_{tot} is the largest scale along the LOS. Since the field is isotropic, it is possible to evaluate this integral changing variables from z_1 and z_2 , to $z_+ = (z_1 + z_2)/2$ and $z_- = z_2 - z_1$. With this new variables, equation B3 becomes

$$\begin{aligned} \langle [V_z(\mathbf{X}_1) - V_z(\mathbf{X}_2)]^2 \rangle &= 2 C_1 \int_0^{z_{tot}} \int_{z_-/2}^{z_{tot} - (z_-/2)} \left[(R^2 + z_-^2)^{m/2} - z_-^m \right] dz_+ dz_- \\ &= 2 C_1 \int_0^{z_{tot}} \left[(R^2 + z_-^2)^{m/2} - z_-^m \right] (z_{tot} - z_-) dz_-. \end{aligned} \quad (\text{B4})$$

The remaining integral can be solved analytically in terms of hypergeometric functions, and converge only for $m > -1$ (which is automatically satisfied since the spectrum is steep therefore with $m > 0$), yielding (a similar formula can be found in Stutzki et al. 1998):

$$\begin{aligned} \langle [V_z(\mathbf{X}_1) - V_z(\mathbf{X}_2)]^2 \rangle &= 2 C_1 z_{tot}^2 \left\{ R^m {}_2F_1 \left(\frac{1}{2}, -\frac{m}{2}, \frac{3}{2}; -\frac{z_{tot}^2}{R^2} \right) + \left(\frac{R^2}{z_{tot}^2} \right) \frac{[R^m - (z_{tot}^2 + R^2)^{m/2}]}{m+2} \right. \\ &\quad \left. - \frac{z_{tot}^m (m+1) + (z_{tot}^2 + R^2)^{m/2}}{m+2} \right\}. \end{aligned} \quad (\text{B5})$$

Where ${}_2F_1$ is the hypergeometric function, with a series expansion (hypergeometric series) of the form:

$$\begin{aligned} {}_2F_1(a, b, c; x) &= y(x) = 1 + \frac{ab}{c} \frac{x}{1!} + \frac{a(a+1)b(b+1)}{c(c+1)} \frac{x^2}{2!} + \dots \\ c &\neq 0, -1, -2, -3, \dots \end{aligned} \quad (\text{B6})$$

However, for all practical purposes, we can calculate it numerically, directly from the definition in equation (B4), yet the zero point (determined by C_1) has to be estimated. At small separations ($R \ll z_{tot}$), the projected structure functions is well approximated by a power-law of the form

$$\langle [V_z(\mathbf{X}_1) - V_z(\mathbf{X}_2)]^2 \rangle \approx C_1' R^{m+1} \quad R \ll z_{tot}. \quad (\text{B7})$$

Where C_1' is a constant that can be related to C_1 by matching the zero point of the 2D structure function from the data to a numerical computation using equation (B3). For large separations ($R \gg z_{tot}$) equation (B5), will follow a power law of the form

$$\langle [V_z(\mathbf{X}_1) - V_z(\mathbf{X}_2)]^2 \rangle \approx C_1'' R^m \quad R \gg z_{tot}. \quad (\text{B8})$$

Where C_1'' is another constant that will depend on the zero point of velocity fluctuations and on z_{tot} as well. If we have enough inertial range below z_{tot} . The spectral index m can be obtained from the 2D structure function, and verified with the power spectrum. An example of a numerically integrated structure function using equation (B4) and the asymptotic in equations (B7) and (B8) is shown in Figure B1 for a structure function index of $m = 2/3$. This first panel is almost equivalent to Figure (3), where we calculate the structure function of integrated data-cubes (Gaussian), but in Figure B1 only theoretical expressions have been used, agreement of the two results provides us with a healthy verification.

B.2. Projection of a field with a shallow power spectrum

Consider a shallow density field (also isotropic), with a 3D structure function of the form (combining eqs. [A4] and [6])

$$\langle (\rho(\mathbf{x}_1) - \rho(\mathbf{x}_2))^2 \rangle = 2 \left[B(0) - C_2 \left(\frac{r}{r_c} \right)^{\eta/2} K_{\eta/2} \left(\frac{r}{r_c} \right) \right]. \quad (\text{B9})$$

The structure function of integrated density (column density) for this case can be written as

$$\langle [I(\mathbf{X}_1) - I(\mathbf{X}_2)]^2 \rangle = 2 C_2 z_{tot} \int_0^{z_{tot}} \left[- \left(\frac{\sqrt{R^2 + z^2}}{r_c} \right)^{\eta/2} K_{\eta/2} \left(\frac{\sqrt{R^2 + z^2}}{r_c} \right) + \left(\frac{z}{r_c} \right)^{\eta/2} K_{\eta/2} \left(\frac{z}{r_c} \right) \right] dz, \quad (\text{B10})$$

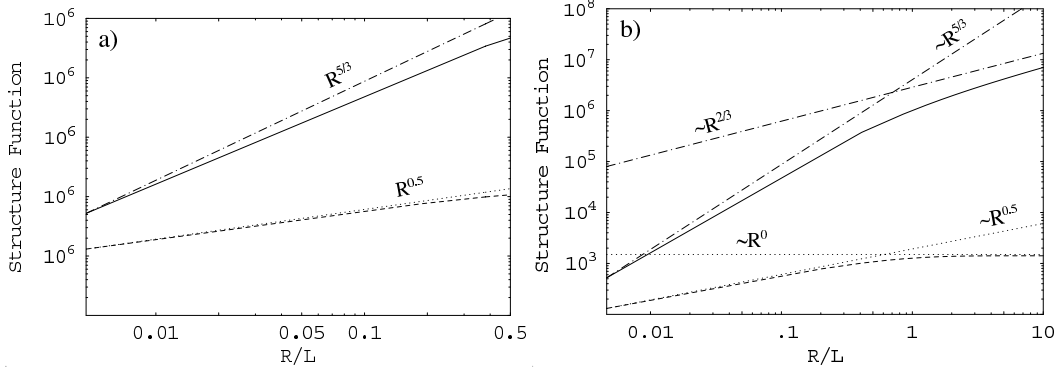


FIG. B1.— Integrated structure functions from a field with a power-law spectrum. a) The *solid* line is the exact result (numerically integrating eq.[B3]) for a field with steep spectrum (3D power spectrum index of $\gamma_{3D} = -11/3$), the *dashed* line is for a shallow spectrum (3D power spectrum index $\gamma_{3D} = -2.5$, obtained numerically integrating eq.[B10]). The *dash-dotted*, are the power-law asymptotics for the steep spectrum, and the *dotted* line for the shallow spectrum. Figure b) is the same as a) but we integrated for separations beyond the thickness of the object (chosen here to be 216 to compare with the Gaussian Cubes in Figure 3), we can see clearly the effect of limited thickness discussed in the text.

where for a shallow spectrum $\eta < 0$. This integral is more difficult to evaluate analytically than the long-wave dominated case, but for practicality we can solve it numerically. We also find that for small scales, the result can be well approximated by a simple power-law:

$$\langle [I(\mathbf{X}_1) - I(\mathbf{X}_2)]^2 \rangle \approx C_2' R^{m+1} \quad R \ll z_{tot}. \quad (B11)$$

Similarly, the zero point can be found by matching the numerical result of eq. (B11) to the calculated (2D) structure function from the data. For large separations ($R \gg z_{tot}$) the resulting structure function of the integrated field will follow the asymptotic scaling of the 3D structure function:

$$\langle [I(\mathbf{X}_1) - I(\mathbf{X}_2)]^2 \rangle \approx \text{constant} = C_2'' R^0 \quad R \gg z_{tot}. \quad (B12)$$

In Figure B1 we also show an example of the numerical calculation of an integrated structure function using (B10) and the asymptotics in equations (B11) and (B12), for an index $\eta = -0.5$ (corresponding to a 3D power spectrum with an index $\gamma_{3D} = -2.5$).

C. POWER SPECTRA OF A FIELD INTEGRATED ALONG THE LINE OF SIGHT

The procedure presented here can be repeated analogously also for a scalar field (e.g. density). Consider the correlation function a velocity, projected along the LOS direction (chosen here to be z):

$$\begin{aligned} \langle V_z(\mathbf{R}) V_z(\mathbf{X} + \mathbf{R}) \rangle &= \left\langle \int dz_1 v_z(\mathbf{x}) \int dz_2 v_z(\mathbf{x} + \mathbf{r}) \right\rangle \\ &= \iint dz_1 dz_2 \langle v_z(\mathbf{x}) v_z(\mathbf{x} + \mathbf{r}) \rangle = \iint dz_1 dz_2 B_{zz}(\mathbf{r}). \end{aligned} \quad (C1)$$

$$\langle V_z(\mathbf{R}) V_z(\mathbf{X} + \mathbf{R}) \rangle = \iint dz_1 dz_2 \langle v_z(\mathbf{x}) v_z(\mathbf{x} + \mathbf{r}) \rangle = \iint dz_1 dz_2 B_{zz}(\mathbf{r}). \quad (C2)$$

Or in terms of the underlying 3D spectrum (inverting equation A5)

$$\langle V_z(\mathbf{R}) V_z(\mathbf{X} + \mathbf{R}) \rangle = \iint dz_1 dz_2 \left[\int d^3 \mathbf{k} e^{i \mathbf{k} \cdot \mathbf{r}} F_{zz}(\mathbf{k}) \right]. \quad (C3)$$

The two-dimensional power spectrum can be obtained taking the Fourier transform of the last expression

$$P_{2D, V_z}(\mathbf{K}) = \frac{1}{4\pi^2} \int d^2 \mathbf{R} e^{-i \mathbf{K} \cdot \mathbf{R}} \left\{ \iint dz_1 dz_2 \left[\int d^3 \mathbf{k} e^{i \mathbf{k} \cdot \mathbf{r}} F_{zz}(\mathbf{k}) \right] \right\}. \quad (C4)$$

And using $\mathbf{k} = (\mathbf{K}, k_z)$, $\mathbf{r} = (\mathbf{R}, z_2 - z_1)$:

$$P_{2D, V_z}(\mathbf{K}) = \frac{1}{4\pi^2} \int d^2 \mathbf{R} e^{-i \mathbf{K} \cdot \mathbf{R}} \left\{ \iint dz_1 dz_2 \left[\int d^3 \mathbf{k} e^{i \mathbf{K} \cdot \mathbf{R} + i k_z (z_2 - z_1)} F_{zz}(\mathbf{K}, k_z) \right] \right\}. \quad (C5)$$

We can interchange the order of integration:

$$P_{2D, V_z}(\mathbf{K}) = \frac{1}{4\pi^2} \iint dz_1 dz_2 \left\{ \int d^3 \mathbf{k}' \left[\int d^2 \mathbf{R} e^{i (\mathbf{K}' - \mathbf{K}) \cdot \mathbf{R} + i k'_z (z_2 - z_1)} F_{zz}(\mathbf{K}', k'_z) \right] \right\}. \quad (C6)$$

After performing the integral over \mathbf{R} one has:

$$P_{2D, V_z}(\mathbf{K}) = \iint dz_1 dz_2 \int d^3 \mathbf{k}' \left[e^{i k'_z (z_2 - z_1)} \delta(\mathbf{K}' - \mathbf{K}) F_{zz}(\mathbf{K}', k'_z) \right]. \quad (C7)$$

Now integrate over \mathbf{K}' :

$$P_{2D,V_z}(\mathbf{K}) = \iint dz_1 dz_2 \left[\int dk_z e^{ik'_z(z_2-z_1)} F_{zz}(-\mathbf{K}, k'_z) \right]. \quad (\text{C8})$$

Changing variables to $z_+ = (z_1 + z_2)/2$, $z_- = z_2 - z_1$, using $F_{zz}(-\mathbf{k}) = F_{zz}(\mathbf{k})$, after of integration in z_- :

$$P_{2D,V_z}(\mathbf{K}) = 4\pi \int dz_+ \left[\int dk_z \delta(k_z) F_{zz}(\mathbf{K}, k'_z) \right]. \quad (\text{C9})$$

Now we do the integral over k'_z , then finally over z_+ :

$$\begin{aligned} P_{2D,V_z}(\mathbf{K}) &= 4\pi \int dz_+ [F_{zz}(\mathbf{K}, 0)] \\ &= 4\pi z_{tot} F_{zz}(\mathbf{K}, 0), \end{aligned} \quad (\text{C10})$$

lastly, replacing $k_z = 0$, in equation (A8) $F_{zz}(\mathbf{K}, 0) = F_{NN}(K)$, we recover from the integrated structure function the spectrum of the solenoidal component of the velocity:

$$P_{2D,V_z}(\mathbf{K}) = 4\pi z_{tot} F_{NN}(K). \quad (\text{C11})$$

D. SECOND ORDER STRUCTURE FUNCTION OF UNNORMALIZED VELOCITY CENTROIDS

Consider the structure function of the unnormalized velocity centroids (equation 21):

$$\langle [S(\mathbf{X}_1) - S(\mathbf{X}_2)]^2 \rangle = \left\langle \left(\alpha \int v_z(\mathbf{x}_1) \rho(\mathbf{x}_1) dz - \alpha \int v_z(\mathbf{x}_2) \rho(\mathbf{x}_2) dz \right)^2 \right\rangle. \quad (\text{D1})$$

As described in §§2.2 (and in Lazarian 1995), we can rewrite last line as in equations (22) and (23), that we rewrite here:

$$\langle [S(\mathbf{X}_1) - S(\mathbf{X}_2)]^2 \rangle = \alpha^2 \iint dz_1 dz_2 [D(\mathbf{r}) - D(\mathbf{r})|_{\mathbf{x}_1=\mathbf{x}_2}], \quad (\text{D2})$$

where

$$D(\mathbf{r}) = \langle (v_z(\mathbf{x}_1)\rho(\mathbf{x}_1) - v_z(\mathbf{x}_2)\rho(\mathbf{x}_2))^2 \rangle. \quad (\text{D3})$$

Using the definitions $v_z = v_0 + \tilde{v}_z$, $\rho = \rho_0 + \tilde{\rho}$ in (D3) we have

$$\begin{aligned} D(\mathbf{r}) &= \langle [v_0\rho_0 + \tilde{v}_z(\mathbf{x}_1)\rho_0 + v_0\tilde{\rho}(\mathbf{x}_1) + \tilde{v}_z(\mathbf{x}_1)\tilde{\rho}(\mathbf{x}_1) - v_0\rho_0 + \tilde{v}_z(\mathbf{x}_2)\rho_0 + v_0\tilde{\rho}(\mathbf{x}_2) + \tilde{v}_z(\mathbf{x}_2)\tilde{\rho}(\mathbf{x}_2)]^2 \rangle \\ &= \langle \{v_0[\tilde{\rho}(\mathbf{x}_1) - \tilde{\rho}(\mathbf{x}_2)] + \rho_0[\tilde{v}_z(\mathbf{x}_1) - \tilde{v}_z(\mathbf{x}_2)] + [\tilde{v}_z(\mathbf{x}_1)\tilde{\rho}(\mathbf{x}_1) - \tilde{v}_z(\mathbf{x}_2)\tilde{\rho}(\mathbf{x}_2)]\}^2 \rangle. \end{aligned} \quad (\text{D4})$$

Expansion of the last expression yields

$$\begin{aligned} D(\mathbf{r}) &= \langle v_0^2 [\rho(\mathbf{x}_1) - \rho(\mathbf{x}_2)]^2 + \rho_0^2 [v_z(\mathbf{x}_1) - v_z(\mathbf{x}_2)]^2 + [\tilde{v}_z(\mathbf{x}_1)\tilde{\rho}(\mathbf{x}_1) - \tilde{v}_z(\mathbf{x}_2)\tilde{\rho}(\mathbf{x}_2)] \\ &\quad + 2v_0\rho_0 [\rho(\mathbf{x}_1) - \rho(\mathbf{x}_2)] [v_z(\mathbf{x}_1) - v_z(\mathbf{x}_2)] + 2\rho_0 [v_z(\mathbf{x}_1) - v_z(\mathbf{x}_2)] [\tilde{v}_z(\mathbf{x}_1)\tilde{\rho}(\mathbf{x}_1) - \tilde{v}_z(\mathbf{x}_2)\tilde{\rho}(\mathbf{x}_2)] \\ &\quad + 2v_0 [v_z(\mathbf{x}_1) - v_z(\mathbf{x}_2)] [\tilde{v}_z(\mathbf{x}_1)\tilde{\rho}(\mathbf{x}_1) - \tilde{v}_z(\mathbf{x}_2)\tilde{\rho}(\mathbf{x}_2)] \rangle \\ &= v_0^2 \langle [\rho(\mathbf{x}_1) - \rho(\mathbf{x}_2)]^2 \rangle + \rho_0^2 \langle [v_z(\mathbf{x}_1) - v_z(\mathbf{x}_2)]^2 \rangle + \langle [\tilde{v}_z(\mathbf{x}_1)\tilde{\rho}(\mathbf{x}_1) - \tilde{v}_z(\mathbf{x}_2)\tilde{\rho}(\mathbf{x}_2)]^2 \rangle + \\ &\quad + 2v_0\rho_0 \langle [\rho(\mathbf{x}_1) - \rho(\mathbf{x}_2)] [v_z(\mathbf{x}_1) - v_z(\mathbf{x}_2)] \rangle + 2\rho_0 \langle [v_z(\mathbf{x}_1) - v_z(\mathbf{x}_2)] [\tilde{v}_z(\mathbf{x}_1)\tilde{\rho}(\mathbf{x}_1) - \tilde{v}_z(\mathbf{x}_2)\tilde{\rho}(\mathbf{x}_2)] \rangle \\ &\quad + 2v_0 \langle [\rho(\mathbf{x}_1) - \rho(\mathbf{x}_2)] [\tilde{v}_z(\mathbf{x}_1)\tilde{\rho}(\mathbf{x}_1) - \tilde{v}_z(\mathbf{x}_2)\tilde{\rho}(\mathbf{x}_2)] \rangle. \end{aligned} \quad (\text{D5})$$

Now consider the cross-terms one by one, the third term in equation (D5) is

$$\langle [\tilde{v}_z(\mathbf{x}_1)\tilde{\rho}(\mathbf{x}_1) - \tilde{v}_z(\mathbf{x}_2)\tilde{\rho}(\mathbf{x}_2)]^2 \rangle = \langle \tilde{v}_z^2(\mathbf{x}_1)\tilde{\rho}^2(\mathbf{x}_1) \rangle + \langle \tilde{v}_z^2(\mathbf{x}_2)\tilde{\rho}^2(\mathbf{x}_2) \rangle - 2 \langle \tilde{v}_z(\mathbf{x}_1)\tilde{\rho}(\mathbf{x}_1)\tilde{v}_z(\mathbf{x}_2)\tilde{\rho}(\mathbf{x}_2) \rangle. \quad (\text{D6})$$

Relating the fourth order moments with the second order using the Millionshikov hypothesis ⁸ (see Monin & Yaglom 1975) $\langle h_1 h_2 h_3 h_4 \rangle \approx \langle h_1 h_2 \rangle \langle h_3 h_4 \rangle + \langle h_1 h_3 \rangle \langle h_2 h_4 \rangle + \langle h_1 h_4 \rangle \langle h_2 h_3 \rangle$ we have

$$\langle \tilde{v}_z^2(\mathbf{x}_1)\tilde{\rho}^2(\mathbf{x}_1) \rangle = \langle \tilde{v}_z(\mathbf{x}_1)\tilde{\rho}(\mathbf{x}_1)\tilde{v}_z(\mathbf{x}_1)\tilde{\rho}(\mathbf{x}_1) \rangle \approx \langle \tilde{v}_z^2(\mathbf{x}_1) \rangle \langle \tilde{\rho}^2(\mathbf{x}_1) \rangle + 2 \langle \tilde{v}_z(\mathbf{x}_1)\tilde{\rho}(\mathbf{x}_1) \rangle^2, \quad (\text{D7})$$

$$\langle \tilde{v}_z^2(\mathbf{x}_2)\tilde{\rho}^2(\mathbf{x}_2) \rangle = \langle \tilde{v}_z(\mathbf{x}_2)\tilde{\rho}(\mathbf{x}_2)\tilde{v}_z(\mathbf{x}_2)\tilde{\rho}(\mathbf{x}_2) \rangle \approx \langle \tilde{v}_z^2(\mathbf{x}_2) \rangle \langle \tilde{\rho}^2(\mathbf{x}_2) \rangle + 2 \langle \tilde{v}_z(\mathbf{x}_2)\tilde{\rho}(\mathbf{x}_2) \rangle^2, \quad (\text{D8})$$

$$\begin{aligned} 2 \langle \tilde{v}_z(\mathbf{x}_1)\tilde{\rho}(\mathbf{x}_1)\tilde{v}_z(\mathbf{x}_2)\tilde{\rho}(\mathbf{x}_2) \rangle &\approx 2 \langle \tilde{v}_z(\mathbf{x}_1)\tilde{\rho}(\mathbf{x}_1) \rangle \langle \tilde{v}_z(\mathbf{x}_2)\tilde{\rho}(\mathbf{x}_2) \rangle \\ &\quad + 2 \langle \tilde{v}_z(\mathbf{x}_1)\tilde{v}_z(\mathbf{x}_2) \rangle \langle \tilde{\rho}(\mathbf{x}_1)\tilde{\rho}(\mathbf{x}_2) \rangle \\ &\quad + 2 \langle \tilde{v}_z(\mathbf{x}_1)\tilde{\rho}(\mathbf{x}_2) \rangle \langle \tilde{v}_z(\mathbf{x}_2)\tilde{\rho}(\mathbf{x}_1) \rangle. \end{aligned} \quad (\text{D9})$$

⁸ Evidently, this hypothesis is identically true for Gaussian fields, strongly non Gaussian fields may show deviations.

If we combine the last three lines using

$$\begin{aligned} \langle [v_z(\mathbf{x}_1) - v_z(\mathbf{x}_2)]^2 \rangle &= \langle \tilde{v}_z^2(\mathbf{x}_1) \rangle - 2 \langle \tilde{v}_z(\mathbf{x}_1) \tilde{v}_z(\mathbf{x}_2) \rangle + \langle \tilde{v}_z^2(\mathbf{x}_2) \rangle \\ &= 2 \langle \tilde{v}_z^2 \rangle - 2 \langle \tilde{v}_z(\mathbf{x}_1) \tilde{v}_z(\mathbf{x}_2) \rangle, \end{aligned} \quad (\text{D10})$$

$$\langle \tilde{v}_z(\mathbf{x}_1) \tilde{v}_z(\mathbf{x}_2) \rangle = \langle \tilde{v}_z^2 \rangle - \frac{1}{2} \langle [v_z(\mathbf{x}_1) - v_z(\mathbf{x}_2)]^2 \rangle, \quad (\text{D11})$$

$$\langle \tilde{\rho}(\mathbf{x}_1) \tilde{\rho}(\mathbf{x}_2) \rangle = \langle \tilde{\rho}^2 \rangle - \frac{1}{2} \langle [\rho(\mathbf{x}_1) - \rho(\mathbf{x}_2)]^2 \rangle. \quad (\text{D12})$$

Together with $\langle \tilde{v}_z(\mathbf{x}_1) \tilde{\rho}(\mathbf{x}_1) \rangle = \langle \tilde{v}_z(\mathbf{x}_2) \tilde{\rho}(\mathbf{x}_2) \rangle = 0$, $\langle \tilde{v}_z^2(\mathbf{x}_1) \rangle = \langle \tilde{v}_z^2(\mathbf{x}_2) \rangle = \langle \tilde{v}_z^2 \rangle$, and $\langle \tilde{\rho}^2(\mathbf{x}_1) \rangle = \langle \tilde{\rho}^2(\mathbf{x}_2) \rangle = \langle \tilde{\rho}^2 \rangle$ equation (D6) reduces to

$$\begin{aligned} \langle [\tilde{v}_z(\mathbf{x}_1) \tilde{\rho}(\mathbf{x}_1) - \tilde{v}_z(\mathbf{x}_2) \tilde{\rho}(\mathbf{x}_2)]^2 \rangle &\approx 2 \langle \tilde{v}_z^2 \rangle \langle \tilde{\rho}^2 \rangle - 2 \langle \tilde{v}_z(\mathbf{x}_1) \tilde{\rho}(\mathbf{x}_2) \rangle \langle \tilde{v}_z(\mathbf{x}_2) \tilde{\rho}(\mathbf{x}_1) \rangle \\ &\quad - 2 \left\{ \left[\langle \tilde{v}_z^2 \rangle - \frac{1}{2} \langle [v_z(\mathbf{x}_1) - v_z(\mathbf{x}_2)]^2 \rangle \right] \right. \\ &\quad \left. \left[\langle \tilde{\rho}^2 \rangle - \frac{1}{2} \langle [\rho(\mathbf{x}_1) - \rho(\mathbf{x}_2)]^2 \rangle \right] \right\}. \end{aligned} \quad (\text{D13})$$

To treat terms of the form $\langle \tilde{\rho} \tilde{v}_z \rangle$ we can generalize the correlation function defined in equation (A1), considering a four-dimensional vector of the form $[v_x(\mathbf{x}), v_y(\mathbf{x}), v_z(\mathbf{x}), \rho(\mathbf{x})]$. The resulting cross-correlation between the z component of the velocity and the density is

$$B_{z\rho}(\mathbf{r}) = \langle v_z(\mathbf{x}_1) \rho(\mathbf{x}_2) \rangle. \quad (\text{D14})$$

Similarly to the derivation of equation (A6) it can be shown that for an isotropic (four-dimensional) field $B_{j\rho}(r) = B_{L\rho}(r)r_j/r$, and $B_{\rho j}(r) = B_{\rho L}(r)r_j/r = -B_{L\rho}(r)r_j/r$. Thus $\langle \tilde{v}_z(\mathbf{x}_1) \tilde{\rho}(\mathbf{x}_2) \rangle = -\langle \tilde{v}_z(\mathbf{x}_2) \tilde{\rho}(\mathbf{x}_1) \rangle$, and equation (D13) simplifies to

$$\begin{aligned} \langle [\tilde{v}_z(\mathbf{x}_1) \tilde{\rho}(\mathbf{x}_1) - \tilde{v}_z(\mathbf{x}_2) \tilde{\rho}(\mathbf{x}_2)]^2 \rangle &\approx 2 \langle \tilde{v}_z(\mathbf{x}_1) \tilde{\rho}(\mathbf{x}_2) \rangle^2 + \langle \tilde{v}_z^2 \rangle \langle [\rho(\mathbf{x}_1) - \rho(\mathbf{x}_2)]^2 \rangle \\ &\quad + \langle \tilde{\rho}^2 \rangle \langle [v_z(\mathbf{x}_1) - v_z(\mathbf{x}_2)]^2 \rangle \\ &\quad - \frac{1}{2} \langle [v_z(\mathbf{x}_1) - v_z(\mathbf{x}_2)]^2 \rangle \langle [\rho(\mathbf{x}_1) - \rho(\mathbf{x}_2)]^2 \rangle. \end{aligned} \quad (\text{D15})$$

The next term of equation (D5)

$$2v_0\rho_0 \langle [\rho(\mathbf{x}_1) - \rho(\mathbf{x}_2)][v_z(\mathbf{x}_1) - v_z(\mathbf{x}_2)] \rangle = 0, \quad (\text{D16})$$

as shown explicitly in Monin & Yaglom (1975). The fifth term in equation (D5) is:

$$\begin{aligned} 2\rho_0 \langle [\tilde{v}_z(\mathbf{x}_1) - \tilde{v}_z(\mathbf{x}_2)][\tilde{v}_z(\mathbf{x}_1) \tilde{\rho}(\mathbf{x}_1) - \tilde{v}_z(\mathbf{x}_2) \tilde{\rho}(\mathbf{x}_2)] \rangle &= 2\rho_0 \langle \tilde{v}_z(\mathbf{x}_1) \tilde{\rho}(\mathbf{x}_1) \rangle + 2\rho_0 \langle \tilde{v}_z(\mathbf{x}_2) \tilde{\rho}(\mathbf{x}_2) \rangle \\ &\quad - 2\rho_0 \langle \tilde{v}_z(\mathbf{x}_1) \tilde{v}_z(\mathbf{x}_2) \tilde{\rho}(\mathbf{x}_1) \rangle \\ &\quad - 2\rho_0 \langle \tilde{v}_z(\mathbf{x}_1) \tilde{v}_z(\mathbf{x}_2) \tilde{\rho}(\mathbf{x}_2) \rangle \end{aligned} \quad (\text{D17})$$

For the terms with correlations of third order we need to introduce the so called two-point third order moments

$$B_{ij,l}(\mathbf{r}) = \langle u_i(\mathbf{x}_1) u_j(\mathbf{x}_1) u_l(\mathbf{x}_2) \rangle. \quad (\text{D18})$$

Which can be generalized to include cross-correlations of density and velocity as explained for equation (D14). Analogously to the second order cross-correlations, considering an isotropic (four-dimensional) field, and decomposing it in terms of longitudinal and lateral components. It can be shown (for more details we refer the reader to Monin & Yaglom 1975) that

$$\langle \tilde{v}_z(\mathbf{x}_1) \tilde{v}_z(\mathbf{x}_2) \tilde{\rho}(\mathbf{x}_1) \rangle = \langle \tilde{v}_z(\mathbf{x}_1) \tilde{v}_z(\mathbf{x}_2) \tilde{\rho}(\mathbf{x}_2) \rangle, \quad (\text{D19})$$

$$\langle \tilde{v}_z(\mathbf{x}_1) \tilde{\rho}_z(\mathbf{x}_1) \tilde{\rho}(\mathbf{x}_2) \rangle = -\langle \tilde{v}_z(\mathbf{x}_1) \tilde{\rho}_z(\mathbf{x}_1) \tilde{\rho}(\mathbf{x}_2) \rangle. \quad (\text{D20})$$

Equation (D19), combined with $\langle \tilde{\rho}(\mathbf{x}_1) \tilde{v}_z^2(\mathbf{x}_1) \rangle = \langle \tilde{\rho}(\mathbf{x}_2) \tilde{v}_z^2(\mathbf{x}_2) \rangle$ reduces equation (D17) to:

$$\begin{aligned} 2\rho_0 \langle [\tilde{v}_z(\mathbf{x}_1) - \tilde{v}_z(\mathbf{x}_2)][\tilde{v}_z(\mathbf{x}_1) \tilde{\rho}(\mathbf{x}_1) - \tilde{v}_z(\mathbf{x}_2) \tilde{\rho}(\mathbf{x}_2)] \rangle &= 4\rho_0 \langle \tilde{\rho}(\mathbf{x}_1) \tilde{v}_z^2(\mathbf{x}_1) \rangle \\ &\quad - 4\rho_0 \langle \tilde{v}_z(\mathbf{x}_1) \tilde{v}_z(\mathbf{x}_2) \tilde{\rho}(\mathbf{x}_1) \rangle. \end{aligned} \quad (\text{D21})$$

Similarly the last term in equation (D5) can be written

$$\begin{aligned} 2v_0 \langle [\rho(\mathbf{x}_1) - \rho(\mathbf{x}_2)][\tilde{v}_z(\mathbf{x}_1) \tilde{\rho}(\mathbf{x}_1) - \tilde{v}_z(\mathbf{x}_2) \tilde{\rho}(\mathbf{x}_2)] \rangle &= 2v_0 \langle \tilde{v}_z(\mathbf{x}_1) \tilde{\rho}^2(\mathbf{x}_1) \rangle \\ &\quad + 2v_0 \langle \tilde{v}_z(\mathbf{x}_2) \tilde{\rho}^2(\mathbf{x}_2) \rangle \\ &\quad - 2v_0 \langle \tilde{\rho}(\mathbf{x}_1) \tilde{\rho}(\mathbf{x}_2) \tilde{v}_z(\mathbf{x}_1) \rangle \\ &\quad - 2v_0 \langle \tilde{\rho}(\mathbf{x}_1) \tilde{\rho}(\mathbf{x}_2) \tilde{v}_z(\mathbf{x}_2) \rangle. \end{aligned} \quad (\text{D22})$$

But in this case, $\langle \tilde{v}_z(\mathbf{x}_1) \tilde{\rho}^2(\mathbf{x}_1) \rangle = \langle \tilde{v}_z(\mathbf{x}_2) \tilde{\rho}^2(\mathbf{x}_2) \rangle = 0$, combined with equation (D20), yields

$$2v_0 \langle [\rho(\mathbf{x}_1) - \rho(\mathbf{x}_2)][\tilde{v}_z(\mathbf{x}_1) \tilde{\rho}(\mathbf{x}_1) - \tilde{v}_z(\mathbf{x}_2) \tilde{\rho}(\mathbf{x}_2)] \rangle = 0. \quad (\text{D23})$$

Finally, combining (D5, D15, D16, D21, D23)

$$\begin{aligned}
D(\mathbf{r}) \approx & v_0^2 \langle [\rho(\mathbf{x}_1) - \rho(\mathbf{x}_2)]^2 \rangle + \rho_0^2 \langle [v_z(\mathbf{x}_1) - v_z(\mathbf{x}_2)]^2 \rangle + 2 \langle \tilde{v}_z(\mathbf{x}_1) \tilde{\rho}(\mathbf{x}_2) \rangle^2 \\
& + \langle \tilde{v}_z^2 \rangle \langle [\rho(\mathbf{x}_1) - \rho(\mathbf{x}_2)]^2 \rangle + \langle \tilde{\rho}^2 \rangle \langle [v_z(\mathbf{x}_1) - v_z(\mathbf{x}_2)]^2 \rangle \\
& - \frac{1}{2} \langle [v_z(\mathbf{x}_1) - v_z(\mathbf{x}_2)]^2 \rangle \langle [\rho(\mathbf{x}_1) - \rho(\mathbf{x}_2)]^2 \rangle + 4\rho_0 \langle \tilde{\rho}(\mathbf{x}_1) \tilde{v}_z^2(\mathbf{x}_1) \rangle \\
& - 4\rho_0 \langle \tilde{v}_z(\mathbf{x}_1) \tilde{v}_z(\mathbf{x}_2) \tilde{\rho}(\mathbf{x}_1) \rangle.
\end{aligned} \tag{D24}$$

Grouping some terms:

$$\begin{aligned}
D(\mathbf{r}) \approx & \langle \tilde{\rho}^2 + \rho_0^2 \rangle \langle [v_z(\mathbf{x}_1) - v_z(\mathbf{x}_2)]^2 \rangle + \langle \tilde{v}^2 + v_0^2 \rangle \langle [\rho(\mathbf{x}_1) - \rho(\mathbf{x}_2)]^2 \rangle \\
& - \frac{1}{2} \langle [v_z(\mathbf{x}_1) - v_z(\mathbf{x}_2)]^2 \rangle \langle [\rho(\mathbf{x}_1) - \rho(\mathbf{x}_2)]^2 \rangle + 2 \langle \tilde{v}_z(\mathbf{x}_1) \tilde{\rho}(\mathbf{x}_2) \rangle^2 \\
& + 4\rho_0 \langle \tilde{\rho}(\mathbf{x}_1) \tilde{v}_z^2(\mathbf{x}_1) \rangle - 4\rho_0 \langle \tilde{v}_z(\mathbf{x}_1) \tilde{v}_z(\mathbf{x}_2) \tilde{\rho}(\mathbf{x}_1) \rangle.
\end{aligned} \tag{D25}$$

And lastly, with $\langle \rho^2 \rangle = \langle \tilde{\rho}^2 + \rho_0^2 \rangle$, and $\langle v^2 \rangle = \langle \tilde{v}^2 + v_0^2 \rangle$ we arrive to equations (24) and (26):

$$\begin{aligned}
D(\mathbf{r}) \approx & \langle \rho^2 \rangle \langle [v_z(\mathbf{x}_1) - v_z(\mathbf{x}_2)]^2 \rangle + \langle v^2 \rangle \langle [\rho(\mathbf{x}_1) - \rho(\mathbf{x}_2)]^2 \rangle \\
& - \frac{1}{2} \langle [v_z(\mathbf{x}_1) - v_z(\mathbf{x}_2)]^2 \rangle \langle [\rho(\mathbf{x}_1) - \rho(\mathbf{x}_2)]^2 \rangle + c(\mathbf{r}),
\end{aligned} \tag{D26}$$

with

$$c'(\mathbf{r}) = 2 \langle \tilde{v}_z(\mathbf{x}_1) \tilde{\rho}(\mathbf{x}_2) \rangle^2 + 4\rho_0 \langle \tilde{\rho}(\mathbf{x}_1) \tilde{v}_z^2(\mathbf{x}_1) \rangle - 4\rho_0 \langle \tilde{v}_z(\mathbf{x}_1) \tilde{v}_z(\mathbf{x}_2) \tilde{\rho}(\mathbf{x}_1) \rangle. \tag{D27}$$

We should note that the second term in equation (D27) has no contribution to the structure function of centroids because when substituted into equation (D2) cancels ($\langle \tilde{\rho}(\mathbf{x}_1) \tilde{v}_z(\mathbf{x}_1)^2 \rangle = \langle \tilde{\rho}(\mathbf{x}_1) \tilde{v}_z(\mathbf{x}_1)^2 \rangle|_{\mathbf{x}_1=\mathbf{x}_2}$). Therefore we omitted this term in the body of the paper. Moreover, this term does not appear in the correlation function of unnormalized centroids, not including it in the definition of $c(\mathbf{r})$ shows better the symmetry between structure functions with correlation functions and spectra.

E. CENTROIDS AND THE “CROSS-TERM” FOR POWER-LAW STATISTICS

We have already discussed the differences between power-law long-wave and short-wave dominated fields (*steep* and *shallow* spectra). In particular, the fact that although in all cases power spectra are power-laws, but structure functions are only power-laws for steep spectra whereas correlation functions are only power-laws (at small scales) for shallow spectra. In this section we will sketch the expectations for the cross-term ($I3[\mathbf{R}]$) for the idealized case of infinite power-law spectra, considering all the different shallow and steep combinations.

E.1. Steep density and steep velocity

In this case the structure function of both fields is well described by a power law. Consider power-law isotropic underlying statistics of the form $d_{v_z}(\mathbf{r}) = C_v r^m$, $d_\rho(\mathbf{r}) = C_\rho r^n$, where $m, n > 0$, and C_v, C_ρ are constants. Here the cross-term will be

$$I3(\mathbf{R}) = -\frac{1}{2} \alpha^2 C_v C_\rho \iint d\mathbf{z}_1 d\mathbf{z}_2 [r^{m+n} - r^{m+n}|_{\mathbf{x}_1=\mathbf{x}_2}], \tag{E1}$$

which is analogous to the projection of a steep field with a spectral index $\gamma_{3D} = -(m+n) - 3$. The resulting cross-term is negative and steeper than both density and velocity. Thus at sufficiently small scales its contribution can be safely neglected compared to the integrated density and velocity.

E.2. Shallow density and steep velocity

Here the structure function of velocity is a power-law $d_{v_z}(\mathbf{r}) \propto C_v r^m$, with $m > 0$ and C_v constant. For small separations (relative to a critical scale r_c as discussed in the main body of the paper) the density fluctuations will have a power-law correlation function $\langle \tilde{\rho}(\mathbf{x}_1) \tilde{\rho}(\mathbf{x}_2) \rangle \approx C_\rho r^n$, where $n < 0$ and C_ρ is constant. Therefore the structure function of density can be presented as $d_\rho(\mathbf{r}) \approx 2\langle \tilde{\rho}^2 \rangle - C_\rho r^n$. For this combination of indices the cross-term becomes

$$I3(\mathbf{R}) \approx -\langle \tilde{\rho}^2 \rangle \langle [V(\mathbf{x}_1) - V(\mathbf{x}_2)]^2 \rangle + \alpha^2 C_v C_\rho \iint d\mathbf{z}_1 d\mathbf{z}_2 [r^{m+n} - r^{m+n}|_{\mathbf{x}_1=\mathbf{x}_2}]. \tag{E2}$$

The first term on the right, although negative has the same slope as $I2(\mathbf{R})$. The two terms inside the integrals are equivalent to the projection of a field with an spectral index $\gamma_{3D} = -(m+n) - 3$. Which in this case is going to be shallower than the velocity, and could be either positive or negative. Positive for $m+n > 0$, and negative for $m+n < 0$. If the level of density fluctuations $\langle \tilde{\rho}^2 \rangle$ is large the first term in the right of eq. (E2) will dominate the slope of $I3(\mathbf{R})$. However such term will be canceled with part of $I2(\mathbf{R})$, changing effectively the weighting of the integrated velocity from $\langle \rho^2 \rangle = \rho_0^2 + \langle \tilde{\rho}^2 \rangle$ to ρ_0^2 . The resulting structure function of unnormalized centroids can be written as⁹

⁹ Equations (E3, E5, and E7) coincide with the decomposition we derived in Ossenkopf et al. (2005).

$$\begin{aligned} \langle [S(\mathbf{X}_1) - S(\mathbf{X}_2)]^2 \rangle &\approx (\nu_0^2 + \langle \tilde{v}_z^2 \rangle) \langle [I(\mathbf{X}_1) - I(\mathbf{X}_2)]^2 \rangle + \rho_0^2 \langle [V(\mathbf{X}_1) - V(\mathbf{X}_2)]^2 \rangle \\ &+ \alpha^2 C_v C_\rho \iint d\mathbf{z}_1 d\mathbf{z}_2 [r^{m+n} - r^{m+n}|_{\mathbf{x}_1=\mathbf{x}_2}] + I4(\mathbf{R}). \end{aligned} \quad (\text{E3})$$

The exact contribution of the terms inside the double integrals to $I3(\mathbf{R})$, and in general the importance of the cross-term to the centroid statistics will depend on the constants C_v and C_ρ . If at large scales the magnitude of the term containing the structure function of integrated velocity and the cross-terms are comparable, then at small scales the centroids could fail tracing velocity.

E.3. Steep Density and shallow velocity

This case is somewhat analogous to that described above. Consider for the density a power-law structure function $d_\rho(\mathbf{r}) \propto C_\rho r^n$, with $n > 0$ and C_ρ constant. For the velocity, a power-law correlation function that translates into a structure function $d_{v_z}(\mathbf{r}) \approx 2(\langle \tilde{v}_z^2 \rangle - C_v r^m)$ with $m < 0$ and C_v constant. We have already discussed that a shallow velocity is not physically motivated. However if we have a steep velocity field without infinite power-law behavior we could have a structure function that resembles the shallow case. For instance if the structure function “saturates” at large separations it will be similar to that of a shallow field, which grows rapidly at small scales and then flattens at large scales. The corresponding cross-term is

$$I3(\mathbf{R}) \approx -\langle \tilde{v}_z^2 \rangle \langle [I(\mathbf{X}_1) - I(\mathbf{X}_2)]^2 \rangle + \alpha^2 C_v C_\rho \iint d\mathbf{z}_1 d\mathbf{z}_2 [r^{m+n} - r^{m+n}|_{\mathbf{x}_1=\mathbf{x}_2}]. \quad (\text{E4})$$

It has a component that scales as the column density (first term on the right). The remaining component could be positive (if $m+n > 0$) or negative (if $m+n < 0$). Unnormalized centroids for these indices can be expressed as

$$\begin{aligned} \langle [S(\mathbf{X}_1) - S(\mathbf{X}_2)]^2 \rangle &\approx \nu_0^2 \langle [I(\mathbf{X}_1) - I(\mathbf{X}_2)]^2 \rangle + (\rho_0^2 + \langle \tilde{\rho}^2 \rangle) \langle [V(\mathbf{X}_1) - V(\mathbf{X}_2)]^2 \rangle \\ &+ \alpha^2 C_v C_\rho \iint d\mathbf{z}_1 d\mathbf{z}_2 [r^{m+n} - r^{m+n}|_{\mathbf{x}_1=\mathbf{x}_2}] + I4(\mathbf{R}). \end{aligned} \quad (\text{E5})$$

E.4. Shallow density and shallow velocity

For this combination of indices we can consider power-law correlation functions (for small separations). Yielding structure functions of the form $d_\rho(\mathbf{r}) \approx 2(\langle \tilde{\rho}^2 \rangle - C_\rho r^n)$, $d_{v_z}(\mathbf{r}) \approx 2(\langle \tilde{v}_z^2 \rangle - C_v r^m)$, with $m, n < 0$, and C_ρ, C_v constants. As a result the cross-term becomes

$$\begin{aligned} I3(\mathbf{R}) &\approx -\langle \tilde{v}_z^2 \rangle \langle [I(\mathbf{X}_1) - I(\mathbf{X}_2)]^2 \rangle - \langle \tilde{\rho}^2 \rangle \langle [V(\mathbf{X}_1) - V(\mathbf{X}_2)]^2 \rangle \\ &- 2\alpha^2 C_v C_\rho \iint d\mathbf{z}_1 d\mathbf{z}_2 [r^{m+n} - r^{m+n}|_{\mathbf{x}_1=\mathbf{x}_2}]. \end{aligned} \quad (\text{E6})$$

Now we have a term that scales as the column density, a term that scales the integrated velocity, and the term inside the integrals (now negative). Notice also that for large values of the velocity or density dispersion, the contribution of column density or integrated velocity respectively is increased within $I3(\mathbf{R})$. But such contributions will be canceled for the unnormalized centroids that will have a structure function:

$$\begin{aligned} \langle [S(\mathbf{X}_1) - S(\mathbf{X}_2)]^2 \rangle &\approx \nu_0^2 \langle [I(\mathbf{X}_1) - I(\mathbf{X}_2)]^2 \rangle + \rho_0^2 \langle [V(\mathbf{X}_1) - V(\mathbf{X}_2)]^2 \rangle \\ &- 2\alpha^2 C_v C_\rho \iint d\mathbf{z}_1 d\mathbf{z}_2 [r^{m+n} - r^{m+n}|_{\mathbf{x}_1=\mathbf{x}_2}] + I4(\mathbf{R}). \end{aligned} \quad (\text{E7})$$

F. CORRELATION FUNCTION AND POWER SPECTRA OF UNNORMALIZED CENTROIDS

Structure functions are considered to be preferable statistics according to Monin & Yaglom (1975). They are subjected to less errors related to averaging. In any case, correlation functions are trivially related to each other by the formula in equation(A4). Using the expression for the structure function of unnormalized centroids from LE03 one gets (see also Levrier 2004 for a direct derivation):

$$\begin{aligned} \langle S(\mathbf{X}_1)S(\mathbf{X}_2) \rangle &\approx \langle \rho^2 \rangle \langle v_z^2 \rangle (\alpha z_{tot})^2 + \alpha^2 \nu_0^2 \iint \langle \tilde{\rho}(\mathbf{x}_1)\tilde{\rho}(\mathbf{x}_2) \rangle d\mathbf{z}_1 d\mathbf{z}_2 + \alpha^2 \rho_0^2 \iint \langle \tilde{v}_z(\mathbf{x}_1)\tilde{v}_z(\mathbf{x}_2) \rangle d\mathbf{z}_1 d\mathbf{z}_2 \\ &+ \alpha^2 \iint \langle \tilde{\rho}(\mathbf{x}_1)\tilde{\rho}(\mathbf{x}_2) \rangle \langle \tilde{v}_z(\mathbf{x}_1)\tilde{v}_z(\mathbf{x}_2) \rangle d\mathbf{z}_1 d\mathbf{z}_2 - \alpha^2 \iint \langle \tilde{\rho}(\mathbf{x}_1)\tilde{v}_z(\mathbf{x}_2) \rangle^2 d\mathbf{z}_1 d\mathbf{z}_2 \\ &+ 2\alpha^2 \rho_0 \iint [\langle \tilde{\rho}(\mathbf{x}_1)\tilde{v}_z(\mathbf{x}_1)\tilde{v}_z(\mathbf{x}_2) \rangle] d\mathbf{z}_1 d\mathbf{z}_2. \end{aligned} \quad (\text{F1})$$

In analogy with equation (27) we can rewrite (F1) as:

$$\langle S(\mathbf{X}_1)S(\mathbf{X}_2) \rangle \approx \langle \rho^2 \rangle \langle v_z^2 \rangle (\alpha z_{tot})^2 + B1(\mathbf{R}) + B2(\mathbf{R}) + B3(\mathbf{R}) + B4(\mathbf{R}), \quad (\text{F2})$$

where

$$B1(\mathbf{R}) = \alpha^2 v_0^2 \iint \langle \tilde{\rho}(\mathbf{x}_1) \tilde{\rho}(\mathbf{x}_2) \rangle dz_1 dz_2, \quad (F3)$$

$$B2(\mathbf{R}) = \alpha^2 \rho_0^2 \iint \langle \tilde{v}_z(\mathbf{x}_1) \tilde{v}_z(\mathbf{x}_2) \rangle dz_1 dz_2, \quad (F4)$$

$$B3(\mathbf{R}) = \alpha^2 \iint \langle \tilde{\rho}(\mathbf{x}_1) \tilde{\rho}(\mathbf{x}_2) \rangle \langle \tilde{v}_z(\mathbf{x}_1) \tilde{v}_z(\mathbf{x}_2) \rangle dz_1 dz_2, \quad (F5)$$

$$B4(\mathbf{R}) = -\alpha^2 \iint \langle \tilde{\rho}(\mathbf{x}_1) \tilde{v}_z(\mathbf{x}_2) \rangle^2 dz_1 dz_2 + 2 \alpha^2 \rho_0 \iint [\langle \tilde{\rho}(\mathbf{x}_1) \tilde{v}_z(\mathbf{x}_1) \tilde{v}_z(\mathbf{x}_2) \rangle] dz_1 dz_2. \quad (F6)$$

Here $B1(\mathbf{R})$ is v_0^2 times the correlation function of fluctuations of column density, $B2(\mathbf{R})$ is $\alpha^2 \rho_0^2$ the correlation function integrated velocity, $B3(\mathbf{R})$ is different from $2I3(\mathbf{R})$ only by a constant, and $B4(\mathbf{R})$ contains the density-velocity cross-correlations found in $I4(\mathbf{R})$.

The Power spectrum of unnormalized centroids is the Fourier Transform of equation (F1):

$$P_{2D,S}(\mathbf{K}) = \langle \rho^2 \rangle \langle v_z^2 \rangle (\alpha z_{tot})^2 \delta(\mathbf{K}) + v_0^2 P_{2D,I}(\mathbf{K}) + \alpha^2 \rho_0^2 P_{2D,V_z}(\mathbf{K}) + \mathcal{F}\{B3(\mathbf{R})\} + \mathcal{F}\{B4(\mathbf{R})\}. \quad (F7)$$

It is interesting of this is that the weighting factors are no longer $\langle v_0^2 + \tilde{v}_z^2 \rangle$ and $\langle \rho_0^2 + \tilde{\rho}^2 \rangle$, but only v_0^2 and ρ_0^2 . And in fact the contribution of the column density alone can be eliminated by removing the mean LOS velocity v_0 . However the cross-term, and density-velocity cross-correlations do affect the scaling properties of the centroids of velocity. And as the turbulence increases in strength and the ratio $\langle \tilde{\rho}^2 \rangle / \rho_0^2$ grows, the “contamination” will also be stronger (see Ossenkopf et al. 2005).

The correlation function of MVCs can be obtained by subtracting $\langle v_z^2 \rangle$ times the correlation function of column density from the correlation function of normalized centroids. Or equivalently:

$$\begin{aligned} CF_{MVC}(\mathbf{R}) &= \langle S(\mathbf{X}_1) S(\mathbf{X}_2) \rangle - \langle I(\mathbf{X}_1) I(\mathbf{X}_2) \rangle \\ &\approx \langle \rho^2 \rangle \langle v_z^2 \rangle (\alpha z_{tot})^2 + B2(\mathbf{R}) + B3'(\mathbf{R}) + B4(\mathbf{R}), \end{aligned} \quad (F8)$$

with

$$\begin{aligned} B3'(\mathbf{R}) &= -\alpha^2 \iint \langle \tilde{\rho}(\mathbf{x}_1) \tilde{\rho}(\mathbf{x}_2) \rangle [\langle \tilde{v}_z^2 \rangle - \langle \tilde{v}_z(\mathbf{x}_1) \tilde{v}_z(\mathbf{x}_2) \rangle] dz_1 dz_2 \\ &= -\frac{\alpha^2}{2} \iint \langle \tilde{\rho}(\mathbf{x}_1) \tilde{\rho}(\mathbf{x}_2) \rangle d_{v_z}(\mathbf{r}) dz_1 dz_2. \end{aligned} \quad (F9)$$

And, thus the power spectrum of MVCs is:

$$P_{2D,MVC}(\mathbf{K}) = \langle \rho^2 \rangle \langle v_z^2 \rangle (\alpha z_{tot})^2 \delta(\mathbf{K}) + \alpha^2 \rho_0^2 P_{2D,V_z}(\mathbf{K}) + \mathcal{F}\{B3'(\mathbf{R})\} + \mathcal{F}\{B4(\mathbf{R})\}. \quad (F10)$$

As the three measures (spectra, correlation, and structure functions) are trivially related, they represent the same statistics. They can be used interchangeably as dictated by practical convenience.

G. UNNORMALIZED CENTROIDS VS. MVCS

When are MVCs better than regular unnormalized centroids? To answer this question let us consider MVCs in terms of correlation functions. First, we can minimize the contribution of density fluctuations to the unnormalized centroids by setting $v_0 = 0$. In this case we can fold the difference of unnormalized and modified centroids in the cross-terms $B3(\mathbf{R})$, and $B3'(\mathbf{R})$ respectively. Thus, the criterion for MVCs to be an improvement over unnormalized centroids would be $|B3(\mathbf{R})| > |B3'(\mathbf{R})|$. In other words:

$$\frac{\left| \iint \langle \tilde{\rho}(\mathbf{x}_1) \tilde{\rho}(\mathbf{x}_2) \rangle \langle \tilde{v}_z(\mathbf{x}_1) \tilde{v}_z(\mathbf{x}_2) \rangle dz_1 dz_2 \right|}{\frac{1}{2} \left| \iint \langle \tilde{\rho}(\mathbf{x}_1) \tilde{\rho}(\mathbf{x}_2) \rangle d_{v_z}(\mathbf{r}) dz_1 dz_2 \right|} > 1. \quad (G1)$$

Let us consider a more realistic *steep* velocity field, with a power-law structure function that saturates at some cutoff scale $r_{v,0}$ (see LP00, Lazarian & Pogosyan 2004):

$$d_{v_z}(\mathbf{r}) = 2 \langle \tilde{v}_z^2 \rangle \frac{r^m}{r^m + r_{v,0}^m}. \quad (G2)$$

We use $r_{v,0}$ to avoid confusion with the critical scale for the short-wave dominated spectra, and because this cutoff scale can also be related to a correlation length for the correlation function:

$$\langle \tilde{v}_z(\mathbf{x}_1) \tilde{v}_z(\mathbf{x}_2) \rangle = \langle \tilde{v}_z^2 \rangle \frac{r_{v,0}^m}{r^m + r_{v,0}^m}. \quad (G3)$$

If we combine this steep velocity field, with a steep density field –i.e. $\langle \tilde{\rho}(\mathbf{x}_1) \tilde{\rho}(\mathbf{x}_2) \rangle = \langle \tilde{\rho}^2 \rangle r_{\rho,0}^n / (r^n + r_{\rho,0}^n)$ –, with the same change of variables as before ($z_- = z_2 - z_1$) the criterion in equation (G1) becomes

$$\frac{\left| \int_0^{z_{tot}} \left[\frac{r_{\rho,0}^n}{(R^2 + z_-^2)^{n/2} + r_{\rho,0}^n} \right] \left[\frac{r_{v,0}^m}{(R^2 + z_-^2)^{m/2} + r_{v,0}^m} \right] dz_- \right|}{\left| \int_0^{z_{tot}} \left[\frac{r_{\rho,0}^n}{(R^2 + z_-^2)^{n/2} + r_{\rho,0}^n} \right] \left[\frac{(R^2 + z_-^2)^{m/2}}{(R^2 + z_-^2)^{m/2} + r_{v,0}^m} \right] dz_- \right|} > 1. \quad (G4)$$

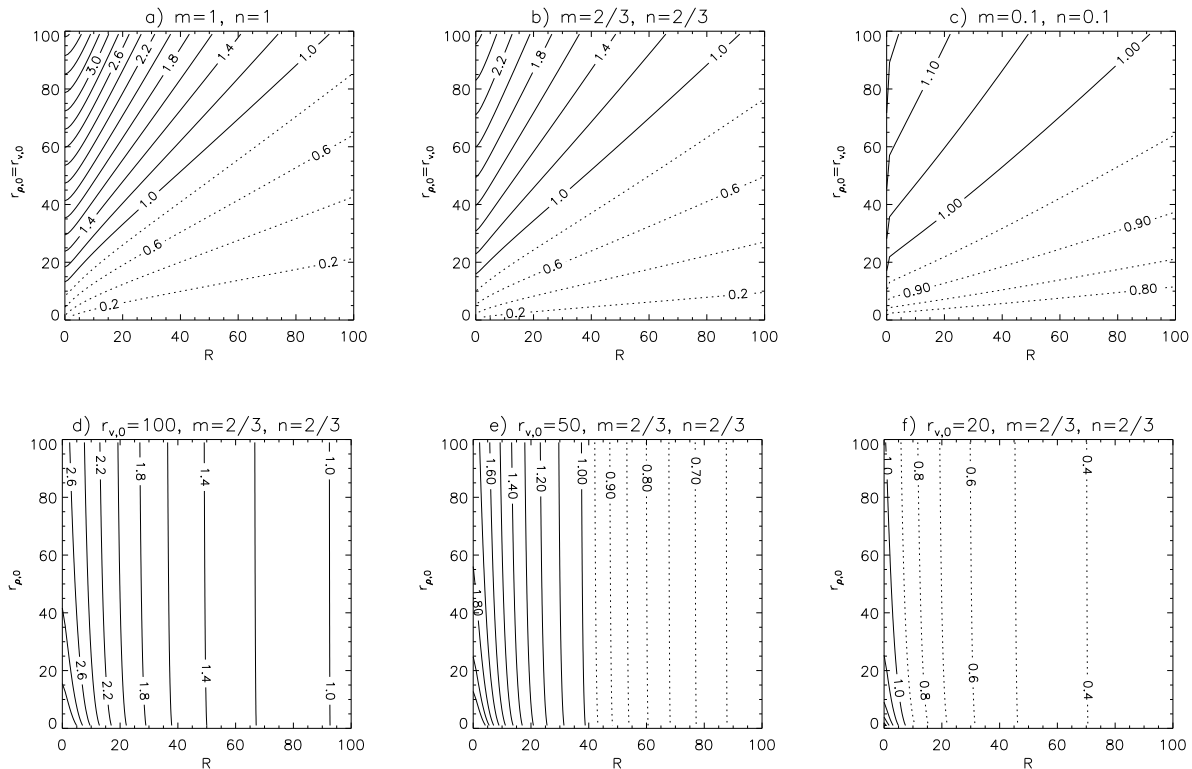


FIG. G1.— Criterion for MVCs to trace velocity better than unnormalized centroids for an example of steep density and velocity. (see equation [G4]). The parameters are labeled in the title and axis for each panel, $z_{\text{tot}} = 100$ in all cases. The criterion is met for parameters that correspond to iso-contours above 1. Panels (a), (b), and (c) show the low sensitivity of the position of the 1 iso-contour with the spectral indices. Panels (d), (e), and (f) show the strong dependence on $r_{v,0}$ and the lag R_y , as well as a weak dependence on $r_{\rho,0}$.

In Figure G1 we plotted iso-contours of this ratio for various combinations of parameters. Within the parameter space corresponding to iso-contour above 1.0 MVCs are expected to trace the statistics of velocity better than unnormalized centroids. In the first three panels (*a*, *b*, *c*) we present, for $r_{\rho,0} = r_{v,0}$ how the ratio in eq.(G4) varies with the lag R over a extreme contrast of possible spectral indices (within the long-wave dominated regime). In the last three panels (*d*, *e*, *f*) we choose a particular set of spectral indices and relax the condition $r_{\rho,0} = r_{v,0}$. In all cases $z_{tot} = 100$. We find that the criterion for MVCs to be better than unnormalized centroids is satisfied for lags smaller than the cutoff for the velocity field, with very little sensitivity to the particular spectral index or the cutoff scale of density.

We performed the same exercise for the other physically motivated case, that is, steep velocity and shallow density. A shallow density can be approximated by the same expression for the correlation function of density, but with a small $r_{p,0}$. We tested for spectral indices from 0.1 to 1.0 for the velocity, and from -1.0 to -0.1 for the density. The same behavior as for the steep-steep case was found. That is, MVC are expected to trace the statistics of velocity better than unnormalized centroids for lags smaller than the velocity correlation-scale ($r_{v,0}$), and smaller than the LOS extent of the object (z_{tot}).

REFERENCES

- Armstrong, J. M., Rickett, B. J., & Spangler, S. R. 1995, *ApJ*, 443, 209
 Bensch, F., Stutzki, J., & Ossenkopf, V. 2001, *A&A*, 366, 636
 Beresnyak, A., Lazarian, A., Cho, J. 2005, *ApJ*, 624, L93
 Brunt, C. M., Heyer, M. H., Vázquez-Semadeni, E., & Pichardo, B. 2003, *ApJ*, 595, 824
 Brunt, C. M., & Heyer, M. H. 2002, *ApJ*, 556, 276
 Brunt, C. M., & Mac Low, M. 2004, *ApJ*, 604, 196
 Cho, J., & Lazarian, A. 2002, *Phys. Rev. Lett.*, 88, 5001
 Cho, J., & Lazarian, A. 2003b, *MNRAS*, 345, 325
 Cho, J., & Lazarian, A. 2005, *Theoretical and Computational Fluid Dynamics*, 19, 127
 Cho, J., Lazarian, A., Vishniac E. T. 2003a, in *Turbulence and Magnetic Fields in Astrophysics*, ed. E. Falgarone, & T. Passot (Berlin: Springer), 53
 Cho, J., Lazarian, A., Vishniac E. T. 2003b, *ApJ*, 595, 812
 Cordes, J. 1999, in *Interstellar Turbulence*, ed. José Franco & Alberto Carramiñana, (Cambridge: Cambridge Univ. Press), p.33
 Deshpande, A. A., Dwarakanath, K. S., & Goss, W. M. 2000, *ApJ*, 543, 227
 Dickman, R. L., & Kleiner, S. C. 1985, *ApJ*, 295, 479
 Esquivel, A., Lazarian, A., Pogosyan, D., & Cho, J. 2003, *MNRAS*, 342, 325
 Heyer, M. H., & Schloerb, F. P. 1997, *ApJ*, 475, 173
 Jackson, J. M., Bania, T. M., Simon, R., Kolpack, M., Clemens, D. P., & Heyer, M. 2002, *ApJ*, 566, L81
 Kitamura, Y., Sunada, K., Hayashi, M., & Hasegawa, T. 1993, *ApJ*, 413, 221
 Kleiner, S. C., & Dickman, R. L. 1985, *ApJ*, 295, 466
 Lai, S., Girart, J. M., & Crutcher, R. M. 2003, *ApJ*, 598, 392
 Larson, R. B. 1981, *MNRAS*, 194, 809
 Larson, R. B. 1992, *MNRAS*, 641
 Lazarian, A. 1995, *A&A*, 293, 507
 Lazarian, A. 1999, in *Plasma Turbulence and Energetic Particles in Astrophysics*, ed. M. Ostrowski, & R. Schlickeiser, (Krakow: Jagiellonian Univ.) , 28
 Lazarian, A. 2003, *Journal of Quantitative Spectroscopy and Radiative Transfer*, 79, 881
 Lazarian, A. 2004, *Journal of Korean Astronomical Society*, 37, 563
 Lazarian, A., & Cho, J. 2005, *Physica Scripta*, T116, 32
 Lazarian, A., & Esquivel, A. 2003, *ApJ*, L37 (LE03)
 Lazarian, A., & Pogosyan, D. 2000, *ApJ*, 537, 72
 Lazarian, A., & Pogosyan, D. 2004, *ApJ*, 616, 943
 Lazarian, A., Pogosyan, D., & Esquivel, A. 2002, in *ASP Conf. Ser. 276, Seeing Through the Dust*, ed. R. Taylor, T. L. Landecker, & A. G. Willis (San Francisco: ASP), 182
 Lazarian, A., Pogosyan, D., Vázquez-Semadeni, E., & Pichardo, B. 2001, *ApJ*, 555, 130
 Lazarian, A., Vishniac, E. T., & Cho, J. 2004, *ApJ*, 603, 180
 Levrier, F. 2004, *A&A*, 421, 387

- Li, D., & Goldsmith, P. F. 2003, *ApJ*, 585, 823
- Matthaeus, W. M., Ghosh, S., Oughton, S., & Roberts, D. A. 1996, *J. Geophys. Res.*, 101, 7619
- Mac Low, M. M., & Ossenkopf, V. 2000, *A&A*, 353, 339
- Miesch, M. S., & Bally, J. 1994, *ApJ*, 429, 645
- Miville-Deschênes, M.-A., Joncas, G., Falgarone, E., & Boulanger, F. 2003a, *A&A*, 411, 109
- Miville-Deschênes, M.-A., Levrier, F., & Falgarone, E. 2003b, *ApJ*, 593, 831
- Müller, W.-C., & Biskamp, D. 2000, *Phys. Rev. Lett.*, 84, 475
- Minter, A. 2002, *ASP Conf. Ser.* 276: Seeing Through the Dust: The Detection of HI and the Exploration of the ISM in Galaxies, 221
- Monin, A. S., & Yaglom, A. M. 1975, *Statistical fluid dynamics: mechanics of turbulence*, Vol. 2., (Cambridge: MIT Press)
- Munch, G. 1958, *Rev. Mod. Phys.*, 30, 1035
- Myers, P. C., & Lazarian, A. 1998, *ApJ*, 507, L157
- Narayan, R., & Goodman, J. 1989, *MNRAS*, 238, 963
- O'Dell, C. R., & Castaneda, H. O. 1987, *ApJ*, 317, 686
- Ossenkopf, V., Esquivel, A., Lazarian, A., Stutzki, J., *A&A*, submitted
- Ossenkopf, V., & Mac Low, M. M. 2002, *A&A*, 390, 307
- Padoan, P., Rosolowsky, E. W., & Goodman, A. A. 2001, *ApJ*, 547, 862
- Padoan, P., Jimenez, R., Nordlund, Å., & Boldyrev, S. 2004a, *Phys. Rev. Lett.*, 92, 191102
- Padoan, P., Jimenez, R., Juvela, M., & Nordlund, Å. 2004b, *ApJ*, 604, L49
- Porter, D., Woodward, P., & Pouquet, A. 1998, *Phys. of Fluids*, 10, 237
- Rosolowsky, E. W., Goodman, A. A., Wilner, D. J., & Williams, J. P. 1999, *ApJ*, 524, 887
- Scalo, J. M. 1984, *ApJ*, 277, 556
- Scalo, J. M. 1987, in *Interstellar Processes*, ed. D. F. Hollenbach & H. A. Thronson (Dordrecht: Reidel), 349
- Spangler, S. R., & Gwinn, C. R. 1990, *ApJ*, 353, L29
- Spoelstra, T. A. T. 1972, *A&A*, 21, 61
- Stanimirović, S., & Lazarian, A., 2001, *ApJ*, 551, 53
- Stenholm, L. G. 1990, *A&A*, 232, 495
- Stutzki, J., Bensch, F., Heithausen, A., Ossenkopf, V., & Zielinsky, M. 1998, *A&A*, 336, 697
- Tafalla, M., Myers, P. C., Caselli, P., & Walmsley, C. M. 2004, *A&A*, 416, 191
- Vázquez-Semadeni, E., Ostriker, E. C., Passot, T., Gammie, C. F., & Stone, J. M. 2000, in *Protostars and Planets IV*, eds. V. Mannings et al. (Tucson: University of Arizona Press), p.3
- Vestuto, J. G., Ostriker, E. C., & Stone, J. M. 2003, *ApJ*, 590, 858
- von Hoerner, S. 1951, *Zeitschrift für Astrophysics*, 30, 17
- Yan, H., & Lazarian, A. 2004, *ApJ*, 614, 757
- Yan, H., Lazarian, A., & Draine, B. T. 2004, *ApJ*, 616, 895
- Zielinsky, M., & Stutzki, J. 1999, *A&A*, 347, 630